A Novel Framework for Acoustic Diagnostic of Artificial Lift System for Oil-Production

by

Sébastien Karim Mannaï
S.M., Massachusetts Institute of Technology, USA (2014)
S.M., École Centrale Paris, France (2013)
S.M., Université de Paris-Saclay, France (2013)

Submitted to the Department of Aeronautics and Astronautics
in partial fulfillment of the requirements for the degree of
Doctor of Philosophy
at the
MASSACHUSETTS INSTITUTE OF TECHNOLOGY
June 2018

Author .. Signature redacted .....
Department of Aeronautics and Astronautics
May 7, 2018

Certified by .. Signature redacted .....
Choon S. Tan
Senior Research Engineer, MIT
Thesis Supervisor

Certified by .. Signature redacted .....
Tianxiang Su
Research Engineer, Schlumberger Doll Research Center
Committee Member

Certified by .. Signature redacted .....
Alexander H. Slocum
Professor of Mechanical Engineering, MIT
Committee Member

Certified by .. Signature redacted .....
Manuel Martinez Sanchez
Professor of Aeronautics and Astronautics Engineering , MIT
Committee Member

Accepted by ..... Signature redacted .....
Hamsa Balakrishnan
Associate Professor of Aeronautics and Astronautics
Chair, Graduate Program Committee

A Novel Framework for Acoustic Diagnostic of Artificial Lift System for Oil-Production

by

Sébastien Karim Mannaï

Submitted to the Department of Aeronautics and Astronautics
on May 7, 2018, in partial fulfillment of the
requirements for the degree of
Doctor of Philosophy

Abstract

Oil extraction on many reservoirs requires the use of rod pump systems to pump the fluid to the surface. A longstanding challenging issue in the operation of rod-pump system is the ability to determine the downhole pump conditions based on the knowledge of a finite set of measurables at the top. A novel acoustic-based diagnostic method is put forward as an enabler for determining the downhole conditions. It consists of reconstructing the pressure signal generated by the pump from an acoustic measurement made at the top. Knowing that the operating pump radiates pressure waves in the fluid, the pump operation can thus be monitored. The physical basis of this acoustic method is demonstrated using results from a model of the rod-pump system complemented by field data measured from representative operating oil wells. The rod pump model has shown to be in good accord with available data. The unique feature differentiating the model formulation from the state of art is that each of the model attributes is linked to the physical process that set the pump operation. The wave equations in the rod string and in the tubing are solved using a custom numerical scheme, and the coupling between the rod and the fluid surrounding it is taken into account. The field measurements and the model results are in accord as they prove the hypothesis that a surface measured pressure can be used to determine the downhole condition of the well. Likewise both the field measurements and the model results provide the physical basis for formulating the scaling rule for generic rod pump system which is used in turn to design a scaled down experimental setup. Specifically, the effect of gas on the pump acoustic signature has been characterized and this general scaling allow one to compare different wells to one another and to obtain a universal scaling parameter to measure the amount of gas in wells pumps. The anticipated technological impact on oil production infrastructure is an acoustic diagnostic framework for assessing a broad class of wells operation, from vertical to horizontal oil wells.

Thesis Supervisor: Choon S. Tan
Title: Senior Research Engineer, MIT

Acknowledgments

This thesis could not have been completed without the assistance and support of my family, advisors, professors, and friends. Above all, I would like to thank my advisor Dr.Tan for his support, patience, and his guidance both in my research and in the classroom for the last 5 years. Thank you for guiding me every day through this endeavor. I am grateful for the support provided by my doctoral committee members and the thesis readers. Thank you Tianxiang for challenging me every week, we had some awesome field trips. My committee and readers provided great constructive feedback so thank you Dr. Pabon, Dr. Campbell and Pr Sanchez. Specifically I would like to to thank Pr Slocum for not only suggesting great ideas, but also for finding me funding for my last semester at MIT. I would also like to thank my numerous mentors, teachers, and coaches from throughout my life. Specifically Sébastien Candel and Jean-Pierre Haigneré, Christophe Laux and Christopher Cripps without whom I would not be at MIT. Walt Pearcy thank you for being an amazing host in Oklahoma and Don Vilines your measurements were very useful. This research has been performed through Schlumberger funding ID 023934-00001. Thank you in particular to Nathan Wicks, Elizabeth Dussan, Francois Auzerais and Sepand Ossia for making this research possible. Additional appreciation goes to all my friends in the GTL especially my officemates David Y, Kevin S, Andras K. And let's not forget to thank Beth and Robin for doing a great administrative work and bearing with all my last minute changes. And finally, special thoughts go out to my parents Nicole and Chawket and my sisters Alexandra, Sabrina and Sophie for their continuous support, encouragement and understanding.

Contents

List of Figures

List of Tables

Nomenclature

α_t Barrel thermal diffusivity

β Fluid compressibility

$\Delta P_{coupler}$ Pressure drop across a coupler

ΔP_{visc} Pressure drop in the well for a viscous steady flow

$\dot{m}$ Mass flow rate

ϵ Strain

γ Heat capacity ratio

Λ Non-linear viscous dissipation coefficient, rod stress wave equation

λ Linear viscous dissipation coefficient, rod stress wave equation

Λ_P Non-linear viscous dissipation coefficient, fluid pressure wave equation

λ_P Linear viscous dissipation coefficient, fluid pressure wave equation

$\mathcal{A}_{pump}$ Pump amplitude, pump stroke

$\mathcal{A}_{top}$ Driving amplitude, unit stroke

$\mathcal{R}$ Pump damping coefficient

$\mathcal{V}_{barrel}$ Barrel volume

μ Fluid dynamic vicosity

μ Fluid dynamic viscosity

ν Fluid kinematic vicosity

ν Fluid kinematic viscosity

Π_i Non dimensional Buckingham-Pi numbers, i integer

ρ Rod density

ρ_f Fluid density

Σ Stress

ξ Longitudinal displacement function

$\xi*$ Longitudinal displacement function normalized by the driving amplitude

$A_{coupler}$ Rod coupler or centralizer cross sectional area

$A_{plunger}$ Pump plunger cross sectional area

A_{rod} Rod cross sectional area

A_{valve} Plunger valve cross sectional area

c Phase velocity in the rod

c_f Phase velocity in the fluid

C_i Integration constants depending on the system geometry, with i integer

CR Pump compression ratio

E Rod Young modulus

e Radial gap between the plunger and the barrel

f Driving frequency

F_0 Fourrier number in the barrel

f_n Primary system resonating frequency

F_{fric} Friction forces applied at the plunger

$F_{viscCouette}$ Viscous forces applied at the plunger by the Couette flow

$F_{viscPoiseuille}$ Viscous forces applied at the plunger by the Poiseuille flow

g Gravity acceleration constant

K Polar radius of gyration of the rod

k Rod stiffness

k' Real part of the wave number

k'' Imaginary part of the wave number

k^{wave} Wave number

l Rod length

$l_{fluid-casing}$ Height of liquid in the casing

$L_{plunger}$ Plunger length

M Lifted fluid mass

m Rod mass

m_{pump} Pump mass

$n_{couplers}$ Total number of couplers/centralizers on the rod string

P_{atm} Atmospheric pressure

P_{casing} Pressure in the casing above any fluid

P_{dyn} Dynamic pressure above the plunger

P_{hydro} Hydrostatic pressure above the plunger

P_{inlet} Pressure at the pump inlet

$P_{plunger+}$ Pressure above the plunger, superscript giving motion direction

$P_{plunger-}$ Pressure below the plunger in the barrel, superscript giving motion direction

P_{tubing} Pressure at the tubing surface, set by the backpressure valve

P_{valve} Pressure lost across a pump valve

r Radial position in the tubing

R_{pipe} Pipe tubing radius

R_{rod} Rod radius

Re Reynolds number in the tubing

T Driving period

t Time

$t*$ Time normalized by the driving period

T_n Primary system resonating period

T_w Primary rod acoustic period

t_{close} Time at which the last valve closed

t^*_{qs} Time normalized radial fluid diffusion time

V Radial fluid velocity in the tubing

V_f Radially averaged fluid velocity in the tubing

v_{rel} Rod-fluid relative velocity

v^*_{rel} Normalized Rod-fluid relative velocity

v_{rod} Rod velocity

x Position along the rod

$x*$ Position along the rod normalized by the rod length

Z Pump impedance

Z_R Resistance part of the pump equivalent impedance

Z_{rod} Rod impedance

Chapter 1

Introduction

1.1 Technical Background

Many oil reservoirs do not generate a pressure high enough to naturally lift the fluid to the earth surface. This is why oil extraction often requires the use of artificial lift systems to pump the fluid to the surface.

There are many different ways to pump the oil to the surface, but rod-pumps are used in about 80% of the wells worldwide and represent a large portion of the oil volume pumped. This statistic shows that they are well suited for low flow rate wells, and as such have to be among the most cost effective methods to extract oil.

Extending the pump performance to meet the needs of a specific engineering mission is an important aspect of artificial lift engineering. As such there is a need to assess and define the engineering attributes/requirements of generic low flow rate artificial lift system for an effective transport of the oil mixture to the surface for a representative oil production site; the proposed research framework for addressing this need includes computations, modeling and experiments on generic fluid-pumping system representative of a fractured producing well.

1.1.1 Rod Pump System Design

A rod pump is used to lift the fluid to the surface when the well pressure is too low. The fluid is lifted to the surface using a positive displacement pump that pushes the fluid upward. That pump is actuated by a long rod (commonly steel) connected to a walking beam at the surface. The walking beam and the gearbox assembly convert a vertical linear motion into a rotational motion. A motor (usually electric) powers the complete system. This work focuses on the dynamics of the rod and downhole assembly. We describe below an ideal pump stroke with only liquid in the plunger. A representative pump system is shown in Figure 1-1.

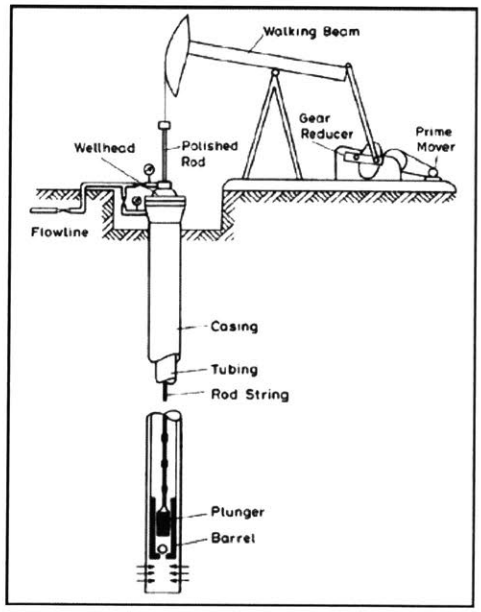

Figure 1-1: A Representative Rod pump system showing the key surface and underground component: plunger, barrel, rodstring, tubing, casing, wellhead, polished rod, walking beam, gear reducer, prime mover.[11]

The downhole pump consists of 4 key components:

- the plunger, acts as a piston
- the barrel, acts as the piston cylinder
- the standing valve, shuts close the barrel on the downstroke, opens it up on the upstroke as seen in Fig 1-2

- the traveling valve, shuts close the plunger on the upstroke, opens it up on the downstroke as seen in Fig 1-3

The fluid accumulates at the bottom of the casing, it is sucked in the pump barrel, it is then pushed upwards in the tubing flowing between the rod and the tubing.

On the upstroke, Fig 1-2, the standing valve is open and the traveling valve is closed. Pulled by the rod the plunger pushes the content of the tubing upward and sucks the well content in the barrel. The long column of liquid in the tubing applies a large pressure on the traveling valve and the plunger.

On the downstroke, Fig 1-3, the rod pushes the plunger downwards, closing the standing valve and opening the traveling valve, allowing the content of the barrel to move above the plunger. The long column of liquid in the tubing now rests on the standing valve, applying a large pressure on it.

The pumped fluid composition varies greatly and depends on the well location but it is usually a mixture of water, oil, various gases, sand, and corrosive chemicals. Because the fluid can be corrosive and carries abrasive particles it is important to keep the pump design simple in order to improve the system reliability, as it usually runs 24/7 for several years.

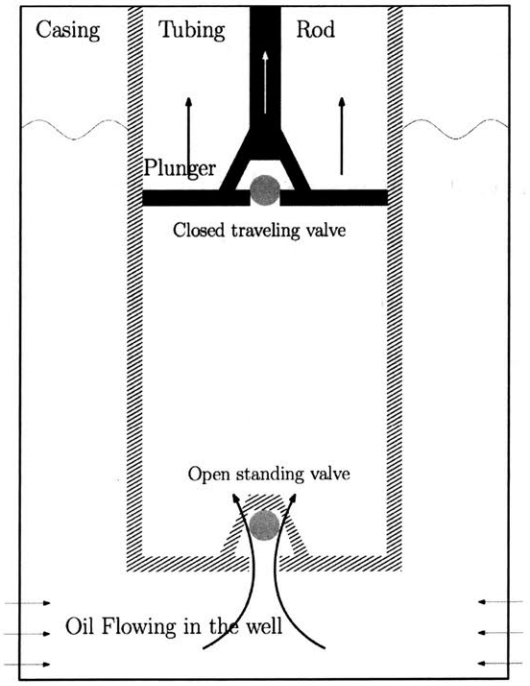

Figure 1-2: Ideal upstroke phase

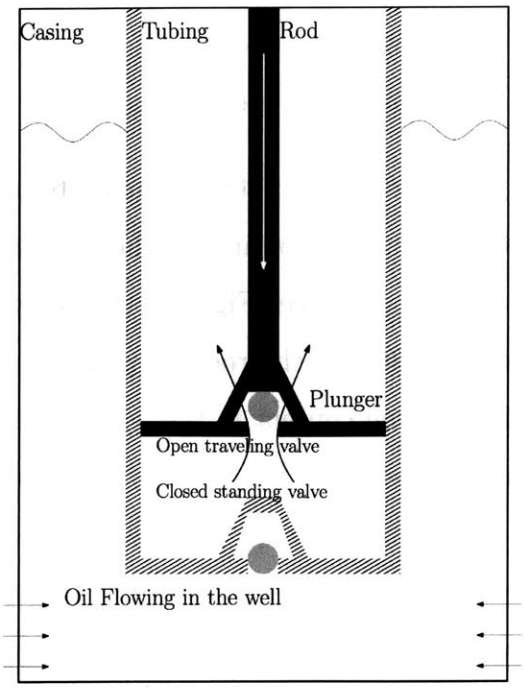

Figure 1-3: Ideal downstroke phase

1.1.2 Rod Pump Characteristics

A rod pump is evaluated based on the following characteristic metrics:

- its mass flow rate
- its efficiency (or power required to operate the system) at each mass flow rate
- the cost of the hardware
- the reliability of the system

The mass flow is usually limited by the amount of fluid the well can provide. If the pump is too fast, the pumped flow becomes larger than the flow provided by the reservoir and once there is no more liquid gas will be pumped. On the downstroke the pump will not be slowed down by viscous incompressible fluid normally in the plunger and will slam into the fluid-gas interface. This increases the stress in the system and can cause premature failure of the rod string or the pump. The system efficiency is linked to the amount of energy used to extract the oil. Consequently this directly affects the cost of each barrel extracted and is of upmost importance. The

cost of the system increases with the amount of material used (the well depth) and the corrosivity of the fluid being pumped (expensive materials may have to be used).

The reliability of the system is highly dependent on the fluid pumped, the well deviation survey (3D profile of the well) and the pumping conditions. Some wells contain highly corrosive and abrasive fluids that will quickly corrode the hardware and the system will deteriorate over time. A non vertical deviated well creates added friction along the rod string or at the pump plunger which limits the hardware lifespan. Some wells can provide a large amount of gas and this may lead to non ideal pumping conditions such as fluid pound, gas interference or gas lock (those terms will be explained in the following chapters). Those conditions reduce the system lifespan. Monitoring those conditions by placing sensors directly at the pump is not realistic since the environment is harsh and that would drive the price of the system in an unreasonable way. Currently, rod stress and displacement measurements are done at the surface. Since the rod is elastic, surface and downhole stress/displacement are not the same when plotted against time. Calculations are therefore implemented to evaluate what is happening at the pump knowing the surface measurements.

1.2 Motivation

The goal for the industry is to develop a system that can analyze the pump operation based on the most simple measurements possible made at the top of the well. Such a system would allow remote operation of the well at a minimal cost. While a conventional rod pump system works well for vertical well, there is a drive towards horizontal and deviated wells that is showing the limits of the current technology. The movements of the rod pump downhole are difficult to infer in deviated wells.

It is especially difficult to infer pump movement using traditional diagnostic and control methods that are based on stress wave analysis of the sucker rod. Quantitative information on pump movement is needed for an effective control of artificial lift system operation. The solid friction between the rod and tubing is difficult to evaluate and is often simply ignored in deviated wells. Furthermore, the well 3D deviation

survey is rarely known, and or any measurements are prone to noise and uncertainties, thus quantifying those forces (between the rod and the tubing) is not an option.

Thus there is a need for an effective way to infer the downhole pump conditions based on the measurements at the top of the well. The downhole conditions pertains to the operation of the pump and its health as well as the fluid composition.

To say this in another way, there is a need for a transfer function that can effectively provide downhole conditions given a finite set of measurables at the top of the well. The transfer function would have a functional dependence on the design attributes of the rod pump system in deviated wells.

1.3 Literature Review

1.3.1 Artificial Lift and Optimization

A good summary of artificial lift technology is given in Brown[17], Neely[18] and Lea [19]. Several teams [20] have attempted to improve some aspects of the rod pump system by changing its motor speed during a stroke.

1.3.2 Rod Model

Rod acoustic has been studied since the 1960's beginning with the seminal work of Sam Gibbs [1]. Dr. Gibbs suggested using the acoustic technique to diagnose pump position using surface position and stress measurements in the rod. Practical system design and pump diagnostic method using the pump chart have been thoroughly discussed by J. Svinos [12]. The theoretical aspects of acoustics are not new and have been expounded upon extensively and in depth in several key books by U. Ingard [7], A.Pierce [4] and J.Lighthill [3]. The applied mathematics necessary to develop a numerical solution of the acoustic system are well known and several well established Galerkin methods were used. The basic fluid mechanics principles necessary to model the various loss processes in internal flow systems have been detailled in the book on Internal Flow [5] and damping models for dynamics systems are given for example by

Kausel[6].

1.3.3 Fluid Acoustic Model

Extensive work has been done on the propagation of pressure pulses in pipes. Specifically the oil industry uses pressure pulses in the mud column to transfer data while drilling from the drill bit to the surface. This mud pulse telemetry system uses pressure pulses at low frequency traveling through two phase flow and has been studied [13]. Substantial resources devoted to developing the rod model were also instrumental in developing the fluid acoustic model largely due to the analogous features in the systems. High frequency acoustic models were initially used in an attempt to model the rod-pump acoustic. Models such as the one developed by Huang[14] were used to understand the effect of cross-sectional changes on pressure pulses: a similar approach has been used by Gerges[15] and Elnemr[16] for muffler acoustic. This approach was initially undertaken; however the rod pump system generates pressure waves that are of low frequencies (less than 10Hz) and as such the techniques tailored to high frequency waves (kHz) are not directly applicable here. The two acoustic boundary types encountered in formulating rod-pump system model are of the nonreflecting and moving boundary type. Alpert[21] and Appelo[24] have addressed and clarified the issue on nonreflecting wave boundary. Corbett [22] and Gaffour [23] modeled the theoretical acoustic effect of a one-dimensional moving acoustic boundary and their work was instrumental in applying this method to model the moving boundary above the plunger in the rod-pump system. The acoustic modeling of the centralizers and couplers was based on the fundamental research in acoustics done by Rienstra[25].

1.4 Research Innovation

The key innovation in this research is in determining the acoustic pressure waves propagating in the fluid and how they are coupled with the stress waves propagating in the lifting rod. An advanced numerical scheme capable of solving the complex coupled non-linear differential equations was developed.

Using the lifting rod as a wave guide has been the industry standard method for the last 30 years. It is a proven method that field engineers know how to analyse and use. However this method has shown its limitations in deviated wells where the lifting rod rubs in the tubing. This alters the measured signal in a way that is not easily modeled thus rendering the results meaningless.
On the other hand, fluid pressure waves are not directly affected by the hole shape or rod-tubing friction. The pressure sensor used to record those waves is also orders of magnitude cheaper and easier to install.

1.5 Research Objective

The overall goal of this research is to define the mutual effect of downhole conditions and well design on the pump system operation (defined in terms of mass flow, efficiency and reliability). Specifically the focus will be on assessing the acoustic characteristic generated by the downhole pump and on field implementable strategy of inferring downhole conditions based on surface acoustic signal. The availability of such a field-implementable strategy allows one to: (1) enhance the effectiveness/efficiency of oil extraction, (2) monitor the health of the system hence increasing the durability/life. Therefore the pump operating characteristics must be inferred from an adequate physical model with a set of finite measurables from sensors at the top of the well used as inputs. A computational supplemented with existing data from oil wells will be undertaken to quantitatively delineate the required attributes of the field-implementable strategy as alluded to above. An anticipated outcome of the research program is enabling the durable operability of non-vertical and deviated wells, which hitherto is confined to vertical wells only. To achieve the goal we set out, we must first address the following research questions:

- What are the parameters characterizing the pump operation, hence the scaling of the system?

- Can the pressure signal at the top of the well be used to infer pump movement

and operating conditions?

- How is the pressure signal affected by the rod string and the rod guides?
- How is the pressure signal affected by the presence of gas in the liquid being pumped?
- How does the well angle affects the rod pump system operation?

Since every oil well is different, it is necessary to define metrics that allow the comparison between wells. Towards this end, scaling a well has been accomplished through two approaches: an analytical model and a more advanced numerical model.

1.6 Research Challenges and Risks

The following are the anticipated challenges and risks in the thesis research.

- The effect of multiphase flow on acoustic damping at low frequencies is unknown
- Potential low signal to noise ratio with relatively high noise level at the surface
- Research results on propagation and transmission of low frequency acoustics in multiphase flow are either non-existent or extrapolated from results for frequencies orders of magnitude higher.

Mitigation of the risks and challenges are offered by the data from Sandia Laboratory acquired in the early 1990's. Several vertical wells were instrumented, with measurements acquired on pressure, position and stress at various depth along the rod string. The wells had various depth, various gas content and actuator with short and long driving amplitude. The Sandia data shows that acoustic pressure signal at the surface is measurable even when the fluid being pump consists of liquid and gas (ie. a multi-phase fluid media). Figure 1-4 show the measured pressure when the fluid being pumped is a single phase liquid only while Figure 1-5 corresponds to a multi-phase situation. . To summarize, even

in a multiphase flow environment a distinct pressure pattern is measurable at the top of the well.

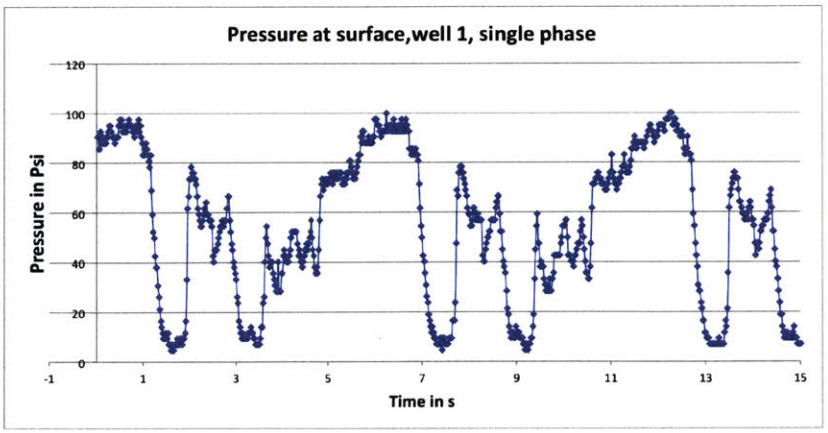

Figure 1-4: Surface pressure in a single phase well

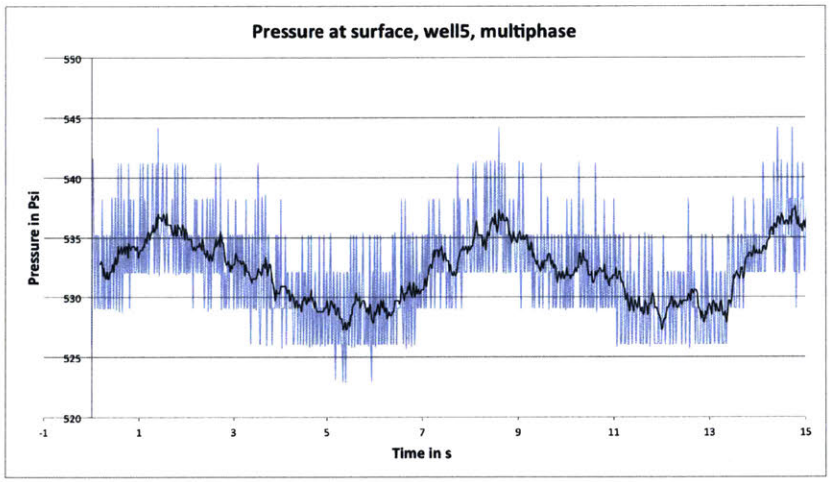

Figure 1-5: Surface pressure in a multiphase phase well with moving average overlaid over raw data to elucidate the pressure variation of interest

1.7 Research Contributions

The contributions consist of the following:

- Formulation of a physically consistent set of equations governing the operation of rod-pump system; each parameter that appears in the equation set can be linked and traced to a physical effect thus eliminating the need of empirical

factors for matching data from operating system in oil fields. This in turn enables the development of a physically consistent model that allows a direct assessment of the influence of the key design parameters on the functionality of system. Thus dynamic similarity of physical effects can be established for experimental assessments of rod pump system operation on a scaled down system implementable in research laboratory environment.

- A universal scaling parameter for rod-pump system operation and design; this constitutes a first-of-a-kind parameter that enable scaling the rod-pump system for oil wells of all types.

- Definition of downhole conditions based on acoustic measurables at the top of the well from horizontal to vertical type.

1.8 Organization of the Thesis

This thesis is organized as follows:

Chapter 2

Chapter two describes the scaling of the system and the resulting key parameters to understand the operation of the pumping system.

Chapter 3

Chapter three provides a detailed analysis of all the forces and the associated loss mechanism occurring in the rod-pump system followed by the equations governing its operation.

Chapter 4

Chapter four provides a detailed analysis of the acoustic dynamics occuring in the fluid, and how those effects affect the dynamics of the rod pump system.

Chapter 5

Chapter five describes the design of an experimental system using the appropriate scaling in order to preserve the system dynamics.

Chapter 6

Chapter six presents the experimental results from the field trip in Oklahoma and an analysis of selected wells.

Chapter 7

Chapter seven presents a summary of the findings as well as recommendation for future work that builds upon the present work.

Chapter 2

Technical Approach

2.1 Introduction

Various complex phenomena can affect the operation of a sucker rod pump system. Since it is impractical and technically difficult to place sensors at the bottom of a real well, an attractive alternative is to instrument the surface of the well.

Thus a model is needed to connect the measurements made at the surface to conditions at the bottom of the real wells. To enable this, a model for the dynamics of the rod pump system has been formulated and developed. There are two versions of the model. The first encompasses the physical complexities and nonlinear behavior of the system; oil well data and experimental measurements are to be used to assess this version of the model. The second version is a simplification of the model whereby closed form solution can be sought for assessing the numerical schemes used to determine the solution of the model governing equations.

The two versions of the model that were developed are both considered to be one dimensional (1D). However the key non-one-dimensional effects are reflected in the physical parameters characterizing the model. A 1D model can provide the required system scaling that reflects several significant rod-pump system operating characteristics.

2.2 Analytical Framework

The rod pump system characterization depends on the dynamic movement of the pump at the bottom of the well. That pump is connected to a walking beam (a rocking beam connected to the main driving motor) at the top of the well with a rod. The walking beam is actuated by a motor and in the context here, it is simply modeled as an actuator system. The movement of the rod is complicated as the movement generated at the top creates axial waves that propagate in the rod before interacting with the pump. The pump then generates pressure waves in the fluid. Thus, fluid, pump and rod characterization constitute a holistic system and must be modeled as a whole.

We will call ξ the longitudinal displacement function of the rod, it depends on the position x and the time t. It indicates the relative position of a fixed point along the rod compared to the resting position. With ϵ as the strain, we have $\epsilon = \frac{\partial \xi}{\partial x}$. If $\frac{\partial \xi}{\partial x}$ is positive then the material is under tensile load and if $\frac{\partial \xi}{\partial x}$ is negative the material is under compressive stress.

While the system will be analysed in details in the following chapters, we will introduced here the simplified equations driving the system and the key scaling parameters that can be extracted from them. Using the driving frequency period T, driving amplitude $\mathcal{A}_{top}$ and the system length l, we can non dimensionalise the time and position coordinates as follows.

$$t = Tt^* \tag{2.1}$$

$$x = lx^* \tag{2.2}$$

$$\xi = \mathcal{A}_{top}\xi^* \tag{2.3}$$

2.2.1 Governing Equation for Rod

The rod movement can be modeled using the wave equation with c the sound velocity in the rod (about 5800m/s for steel) and g the acceleration due to gravity.

$$\frac{\partial^2 \xi}{\partial t^2} = c^2 \frac{\partial^2 \xi}{\partial x^2} + g \tag{2.4}$$

Upon rearranging and using ()* to denote dimensionless variables in the wave equation, we obtain :

$$\frac{\partial^2 \xi^*}{\partial t^{*2}} = \left(\frac{cT}{l}\right)^2 \frac{\partial^2 \xi^*}{\partial x^{*2}} + \frac{gT^2}{\mathcal{A}_{top}} \tag{2.5}$$

The system is initially at rest with no velocities, with a rod stretch due to its own weight. The top boundary is imposed by the pumpjack actuator, while the bottom boundary is the pump, detailed below.

2.2.2 Governing Equation for Pump

We next proceed to elaborate on the boundary condition at the bottom of the rod. The pump has a mass m_{pump} and an area $A_{plunger}$. The rod above the pump has a young modulus E and a cross sectional area A_{rod}. Newton second law is applied at the pump, we obtain the boundary equation at the bottom of the well. The pump acceleration is equal to the sum of the rod stretch force, the pressure force balance across the plunger, friction forces and the pump weight.

$$m_{pump}\frac{\partial^2 \xi}{\partial t^2}(l,t) = -EA_{rod}\frac{\partial \xi}{\partial x} + A_{plunger}\left(P_{plunger+} - P_{plunger-}\right) + F_{fric} + m_{pump}g \tag{2.6}$$

The pressure above $P_{plunger+}$ and below $P_{plunger-}$ the pump plunger must be evaluated as well as the term F_{fric} which contains all the friction and viscous forces applied to the pump. As a first approach, since the pressure above the pump is the hydrostatic pressure while the pressure below the pump is the casing pressure, we have

$P_{plunger+} >> P_{plunger-}$. We assume the fluid of density ρ to be compressible and no pressure waves are reflected at the surface, such that $P_{plunger+} = \rho_f g l + \rho_f c_f \frac{\partial \xi}{\partial t}(l,t)$. The pressure above the plunger is equal to the sum of the hydrostatic pressure and the radiative pressure, this last term indicates the pressure created by radiating pressure waves in the tubing. We also ignore the viscous friction forces at the pump since they are negligible compare to the radiation losses. This simplified boundary conditions does not take into account multiple wave reflections, and is only used in the simplified analytical model, not in the computational model. The pump weight is also minuscule compare to the fluid weight so it can be ignored. Upon rearranging the terms and using ()* to denotes dimensionless variables, and defining the rod stiffness $k = \frac{EA_{rod}}{l}$ and the fluid resistive impedance at the pump $Z_R = A_{plunger}\rho c_f$ we obtain:

$$\frac{m_{pump}}{kT^2}\frac{\partial^2 \xi^*}{\partial t^{*2}}(l,t) = -\frac{\partial \xi^*}{\partial x^*}(l,t) + \frac{m_{fluid}g}{k\mathcal{A}_{top}} + \frac{Z_R}{kT}\frac{\partial \xi^*}{\partial t^*}(l,t) \tag{2.7}$$

2.3 Scaling the System: Buckingham- Pi Coefficients

We have obtain two equations corresponding to the wave propagation and pump boundary condition. We next proceed to use this set of equations in conjunction with Buckingham-Pi Theorem to formulate a set of one-dimensional characterizing parameters.

According to the Buckingham Pi Theorem, we have 12 different quantities (ξ, x, t, l, $\mathcal{A}_{top}$, T, c, g, k, m_{pump}, m_{fluid}, Z_R) and 3 fundamental units (mass, length and time) so we should have 9 dimensionless numbers.
The first 4 come from our unit of measurement:

$$\Pi_1 = \frac{\xi}{\mathcal{A}_{top}} \tag{2.8}$$

$$\Pi_2 = \frac{x}{l} \tag{2.9}$$

$$\Pi_3 = \frac{t}{T} \tag{2.10}$$

$$\Pi_4 = \frac{\mathcal{A}_{top}}{l} \tag{2.11}$$

From the wave equation of the rod-pump system, the following non-dimensional parameters can be extracted. A number that is key for scaling the wave propagation is the ratio of the system characteristic wavelength over its length. It is interesting to note that if we consider the rod as an ideal spring with all the mass suspended at the end we find the same non dimensional frequency $T\sqrt{(\frac{k}{m})} = T\sqrt{(\frac{EA_{rod}}{l}\frac{1}{\rho A_{rod} l})} = \Pi_5$. For a typical deep 3000m well with a steel rod string and a 10s driving period we find $\Pi_5 \approx 20 >> 1$ which would lead us to infer that the rod is not an acoustic system but an elastic one. However the valve opening and closing time, which is critical in determining the motion dynamics, takes a fraction of a second. We now find $\Pi_5 \approx 1$ showing the need for an acoustic model.

$$\Pi_5 = \sqrt{\frac{E}{\rho}}\frac{T}{l} = \frac{cT}{l} \tag{2.12}$$

The gravity term also provides us a number, however it is of limited use.

$$\Pi_6 = \frac{gT^2}{\mathcal{A}_{top}} \tag{2.13}$$

Π_7 given below is an important number and is the ratio of the rod stretch due to the fluid mass by the driving amplitude.

$$\Pi_7 = \frac{m_{fluid}g}{k\mathcal{A}_{top}} \tag{2.14}$$

The last two numbers come from the boundary condition: Π_8 scales the reactance of the pump divided by the rod ideal mechanical impedance.

$$\Pi_8 = \frac{m_{pump}}{kT^2} \tag{2.15}$$

The last number scales the resistive part of the downhole impedance divided by

the rod ideal mechanical impedance.

$$\Pi_9 = \frac{Z_R}{kT} \tag{2.16}$$

2.4 Summary

Equations and boundary conditions that govern the operation of a rod pump system have been formulated, the non-dimensional equivalence of these equations has also been derived to yield a set of key non-dimensional parameters. The attributes of those numbers has been delineated and they will be leveraged upon in the following chapters on various technical aspects of the rod-pump system.

Chapter 3

Rod and Pump System Modeling

3.1 Introduction

In this chapter the system dynamics and physics of the flow inside the well will be discussed and analyzed. Various assumptions on the flow are made and justified. The goal is to have an understanding of the flow inside the well in order to evaluate the various dampings created by the viscous flow. As detailed in Appendix A, the wave equations 3.1 in the rod is key in establishing the link between the movement imposed at the surface and the actual pump movement. The rod longitudinal displacement ξ depends on the propagation of stress waves which travel at a velocity c. Those waves are damped proportionally to the rod velocity and quadratically to the rod relative velocity compare to the fluid. Those damping respectively depend on the constants λ and Λ.

$$\frac{\partial^2 \xi}{\partial t^2}(x,t) = c^2 \frac{\partial^2 \xi}{\partial x^2}(x,t) + \lambda \frac{\partial \xi}{\partial t}(x,t) + \Lambda(\frac{\partial \xi}{\partial t}(x,t) - V_f(x,t))^2 + g \qquad (3.1)$$

However in order to solve the resulting governing equation, the various system damping parameters and the appropriate boundary conditions imposed both at the top and bottom of the rod have to be evaluated. The governing equations of the flow will be detailed and the various damping coefficients will be calculated.

3.2 System Frequencies

The system dynamics consist of physical events that are each associated with a different time scale. The system responds at frequencies that are different from that of the imposed one during its transient regime, so that every stroke constitutes a new transient regime (ball valve non-linearity). As such we have to determine the various time scales that exist. These system time scales are delineated below.

3.2.1 Imposed Motion Frequency

The rod pump is power by an actuator at the top of the well. The actuator imposes a displacement to the top of the rod (called the polished rod). While the displacement is not perfectly sinusoidal the movement can be quantified in terms of a Fourier series. Since the movement of the polished rod is often close to a sinusoidal one, the first component dominates. We will call the imposed period T, with T usually between 6 and 10 seconds. The frequency f is thus given as f=1/T. This quantity was non-dimentionalized in the previous chapter to yield the familiar reduced frequency.

3.2.2 Rod Natural Frequency

The rod stretch is proportional to the stress in the elastic regime. This is always the case in a properly designed system as the rod life is drastically shortened if plastic deformations occurs. Because of that linear relationship between stress and strain, the rod acts as a spring with a distributed mass. In addition the rod of mass m is also lifting the fluid mass M on the upstroke. Thus the system can be described on a lumped parameter basis as a mass-spring system.

Using the lumped parameter model and Hamiltonian mechanics we can evaluate the natural period T_n (and frequency f_n) of the system knowing the rod stiffness $k = \frac{EA_{rod}}{l}$ which is a function of the rod length l, Young Modulus E and cross-sectional area A_{rod}. m is the rod mass and M the lifted fluid and pump mass. As expected since the rod (acting as a spring) mass is distributed it has a lower (1/3)

contribution than the fluid mass [6].

$$T_n = 2\pi\sqrt{\frac{M + m/3}{k}} = 2\pi\sqrt{\frac{M + m/3}{EA_{rod}/l}} \tag{3.2}$$

The rod mass contributes to only a third of the lifted mass as its mass is distributed along its length. The difference in weight lifted on the upstroke and on the downstroke creates two distinct natural frequencies. T_n is estimated to be between 1 and 5 seconds for a representative well.

3.2.3 Longitudinal Modal Frequency

Sound waves travel in the rod at a velocity c that depends on the rod material. Since the rod length is known, we can calculate the associated wave period as:

$$T_w = \frac{l}{c} = \frac{l}{\sqrt{E/\rho}} \tag{3.3}$$

Since c in steel is about 6000m/s and the well length l is usually between 600 and 3000m we find that T_w is between 0.1 and 0.5 seconds or a corresponding frequency f_w between 2Hz and 10Hz. This period is an order of magnitude smaller than the imposed frequency so that the longitudinal waves constitute the high frequency perturbations.

The same type of waves exists in the fluid, except the sound velocity in water is about 1500m/s so the associated longitudinal frequencies are four times lower.

3.3 Tubing Flow

The displacement pump at the bottom of the well string creates a positive (i.e towards the surface) flow on both upstroke and downstroke (see Figure 1-2 and 1-3). The velocity profile of the flow in the tubing will be evaluated in this section. The flow is assumed to be steady state and incompressible. This will allow us to elucidate how the average damping values for the rod wave equation are estimated. Those values are used in the computational model in which many of the assumptions are removed.

3.3.1 Flow Assumption

Several key assumptions are made in order to evaluate the pressure above the pump at the bottom of the tubing (above the piston in Figure 3-4). We will elaborate on the approximations that can be made to facilitate the estimation of the system parameters. The fluid is assumed to be homogenous, viscous and a liquid. The fluid is not modeled as an emulsion, and the presence of gas can be taken into account in the computational model by changing the fluid compressibility, i.e. there is no multiphase flow involving liquid and gas. This is justified by looking at the solubility of methane, which usually is more than 90% of the gas we find, in brine of various salt content as a function of pressure [26].

The flow will be assumed to be fully developed, axisymmetric and quasi steady in order to compute the damping coefficients, i.e. they are independent of the position along the rod.

Geometry and General Assumptions

The fluid flows in a coaxial shaped gap formed by the tubing on the outside and the rod on the inside. While in reality the rod is not always centered, we will assume we have a symmetric geometry. The weighted averaged rod radius is used in tapered wells. The effect of various obstacles such as centralizers or couplers on the flow profile is not taken into account as their length represent at most less than 1% of the well length. However the drag component they create is modeled.

Quasi Steady Flow

We will show that, as a first assumption, we can assume that any change in velocity at the pump is instantly propagated along the tubing. This means that we can analytically calculate the pressure drop along the rod string. We will show that this pressure drop is applied at the pump and is proportional to the pump velocity, thus acting as a damping term. An incompressible flow has an infinite sound velocity and is by definition quasi steady. Therefore the quasi steady assumption is not as

restrictive as the incompressible flow one.

$$Re = \frac{\rho_f V_f D}{\mu} \tag{3.4}$$

The Reynolds number in the tubing is between 0 and 10 000 (for water pumped at a velocity between 0m/s and 1m/s with a hydraulic diameter D of 1cm). Thus the flow is laminar at low Reynolds and can transition to a turbulent flow with increasing Reynolds number. The flow will be assumed to be laminar. As such the fluid flow occurring in a rod pump system can be reasonably approximated as a Couette flow, a Poiseuille flow, or a superposition of both. The Couette and Poiseuille flow profiles are illustrated in Figure 3-1.

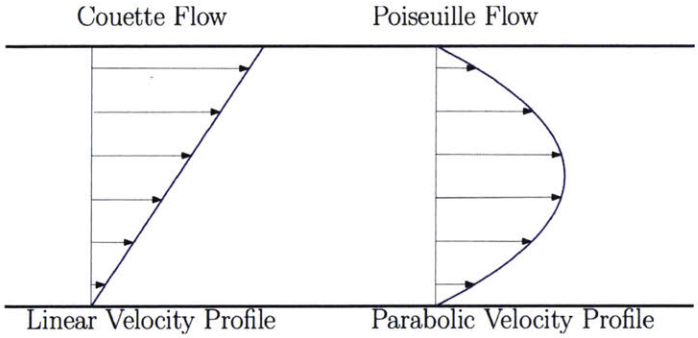

Figure 3-1: Couette Flow driven by the wall and Poiseuille Flow driven by a pressure difference

Comparing the time scale t necessary for a Couette flow and for a Poiseuille flow to reach steady state with the driving period we can establish if the flow is quasi steady or not. If that time t^*_{qs} is significantly smaller than the period of the pump T, then we can consider the flow of the fluid to be quasi steady, i.e. the fluid velocity profile immediately adjusts to the new boundary condition as it changes over time. We define the non dimensional fluid time scale t^*_{qs} using the kinematic viscosity ν of water and the hydraulic radius R.

$$t^*_{qs} = \frac{\nu t}{R} \tag{3.5}$$

Using the results from Muzychka [9] shown in 3-2, we can infer that the non

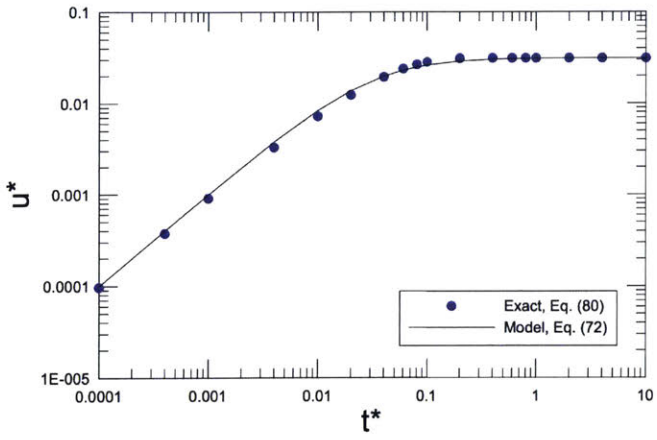

Figure 3-2: Non-dimensional velocity u^* vs non-dimensional time t^*_{qs} for a circular tube [9]

dimensional time t^*_{qs} for the Poiseuille flow to reach 90% of the steady state velocity is 0.1 for a circular tube.

For the Couette flow we find a smaller time $t^*_{qs} = 0.05$. Using the maximum value of t (worst case scenario as the Poiseuille flow takes more time to reach a steady state), we find: $\frac{t}{T} = 0.1 << 1$

Thus the flow encountered in the operation of the rod pump system can be taken to be quasi steady.

Fully Developed Flow

In the vicinity of the pump the flow is not fully developed. However after a few diameters away from the pump, the fluid flow in the tubing is an axisymmetric Poiseuille flow as illustrated in Figure 3-3; the flow profile only depends on the radial coordinate.

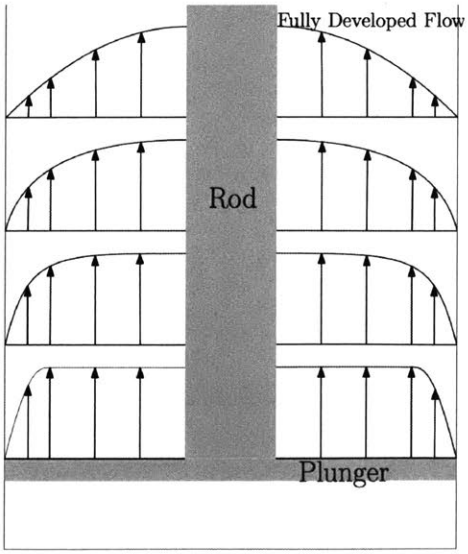

Figure 3-3: Flow reaching its fully developed velocity profile

3.3.2 Velocity profile and Pressure Drop

We will now determine the relation between the flow and the pressure drop in response to overcoming the viscous force along the tubing.

Pumping occurs both on the upstroke and on the downstroke. On the upstroke the plunger pushes upwards the fluid in the tubing. It is also important to take into account the pumping that occurs on the downstroke which is typically about 10% of the volume pumped on the upstroke. As the plunger falls down, the rod is pushed into the barrel cavity thus displacing a fluid volume equal to the rod volume. This creates a pumping action as the rod pushes fluid out of the barrel cavity as illustrated in Figure 3-4.

We begin by estimating the mean fluid velocity profile in the coaxial shaped rod and tubing assembly. The Navier-Stokes equation governing the flow can be written in cylindrical coordinates (r is radial, x is axial) as:

$$\frac{\rho_f}{\mu}\left(\frac{1}{r}\frac{\partial}{\partial r}\left(r\frac{\partial V}{\partial r}\right)\right) = \frac{1}{\mu}\frac{\partial P}{\partial x} - \frac{\rho_f g}{\mu} \tag{3.6}$$

where we have assumed an axisymmetric steady flow. We can decompose P into three components. A hydrostatic pressure such that $\rho_f g = \frac{\partial P_{hyro}}{\partial x}$, a pressure term P_{visc}, set

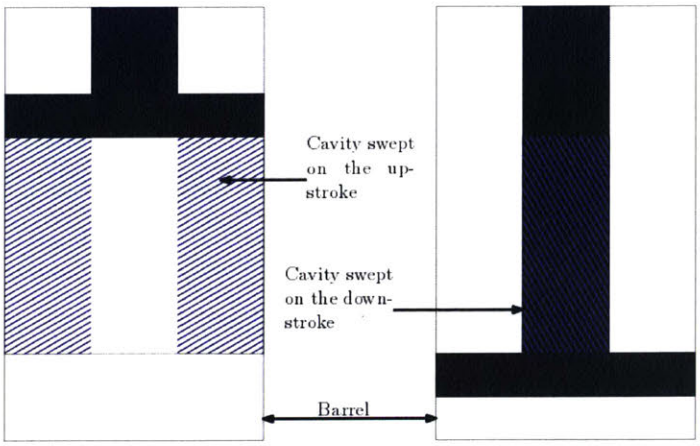

Figure 3-4: Volume swept out by the pump on the up and downstroke

by the viscous Poiseuille flow, and a dynamic pressure term $\rho\frac{\partial V}{\partial t} = -\frac{\partial P_{dyn}}{\partial x}$. Assuming the flow to be quasi-steady, the dynamic pressure then depends on the acceleration of the whole fluid system. P_{visc} is the pressure lost in the complete tubing due to the fluid being viscous.

At the tubing wall of radius R_{pipe} the velocity is zero $V(R_{pipe}) = 0$, and the fluid velocity is equal to the rod velocity (no slip) at R_{rod}. The rod velocity V_{rod} is assumed to be the geometric average of its velocity at the top and bottom such that $V_{rod} = \bar{V}_{rod}$.

Upon integrating equation 3.6, using the boundary conditions as stated above we obtain the main velocity profile V(r,t) as:

$$V(r,t) = \frac{\Delta P_{visc}(t)}{4l\mu}\left((r^2 - R_{pipe}^2) + (R_{pipe}^2 - R_{rod}^2)\frac{ln\left(\frac{r}{R_{pipe}}\right)}{ln\left(\frac{R_{rod}}{R_{pipe}}\right)}\right) + \bar{V}_{rod}\frac{ln\left(\frac{r}{R_{pipe}}\right)}{ln\left(\frac{R_{rod}}{R_{pipe}}\right)} \tag{3.7}$$

V is the fluid velocity, ΔP_{visc} is the difference in pressure between the top and the bottom of the well without the hydrostatic pressure and μ is the fluid viscosity. Figure 3-5 indicates the flow profile according to equation 3.6 in the tubing during the upstroke phase.

The mass flow rate in the pipe is calculated knowing the pump plunger velocity $\dot{\xi}(l,t)$ and the plunger area.

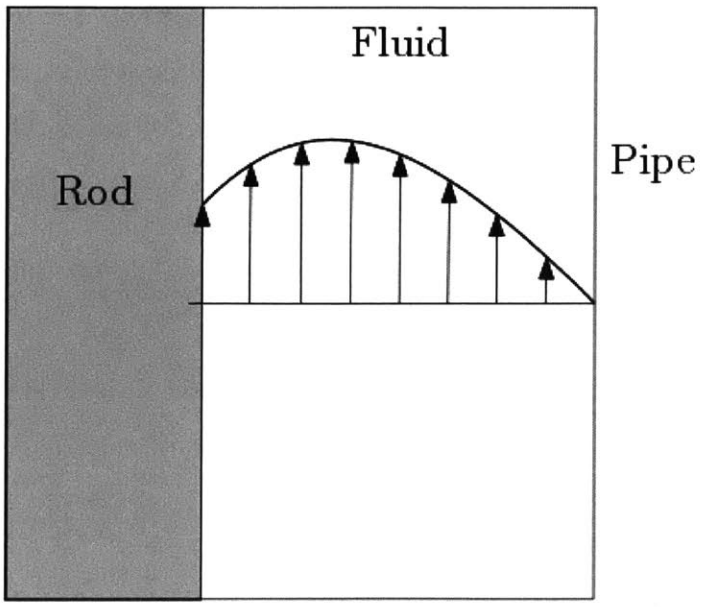

Figure 3-5: A sketch to illustrate the radial variation in fluid flow velocity profile with the rod in the middle. The flow is symmetric around the axis created by the rod. The fluid velocity is 0 on the tubing wall is is equal to the rod velocity at the rod wall

$$\dot{m}(t) = \rho_f A_{plunger} \dot{\xi}(l,t) = 2\pi\rho_f \int_{R_r}^{R_p} rV(r)dr \tag{3.8}$$

Using the velocity profile and the mass flow equation, we can solve for ΔP_{visc}:

$$\Delta P_{visc} = \mu l \frac{R_p^2 - R_r^2 + C_2/2}{C_1} \dot{\xi}(l,t) + \mu l \frac{C_2}{2C_1} \dot{\xi}(0,t) \tag{3.9}$$

Where the geometric coefficients C_1 and C_2 have a functional dependence on the rod and pipe radii.

ΔP_{visc} is proportional to the pump velocity, and can be interpreted as a damping force at the pump. The pressure necessary to pump the fluid also scales with the rod velocity since the rod itself can act as a pump by applying shear stress to the fluid. This depends on the plunger size. A plunger smaller than the tubing will induce a small mass flow and the rod will have a pumping effect. A larger plunger will induce a larger mass flow with a higher average velocity. The pressure difference is also proportional to the well length l and the fluid viscosity μ.

When the fully coupled model is implemented there is no need to calculate analytically the mass flow or the pressure drop ΔP_{visc} as the fluid is taken to be compressible and those values depend on the position along the rod. However for the range of reduced frequency encountered here the quasi-steady modeling can be used to estimate the average damping on the system dynamics.

3.4 Pump Flow: the rod bottom boundary condition

The forces acting on the plungers drive the dynamics of the system and dominate any other effect. It is therefore important to model the pump in details. The pressure $P_{plunger+}$ above and $P_{plunger-}$ below the plunger must be evaluated throughout the cycle. The pump ideal working condition is described, with no gas or potential mechanical issues.

3.4.1 Pressure above the plunger

The pressure above the plunger $P_{plunger+}$ is decomposed into several components:

- Hydrostatic Pressure
- Dynamic Pressure
- Viscous Pressure

The hydrostatic pressure is equal to the pressure at the surface P_{tubing} (imposed by the operator) and the vertical hydrostatic component of the fluid column $\rho_f g l_{fluid}$. The dynamic pressure $P_{dynamic}$ is equal to the pressure necessary to accelerate the fluid. If we assume the fluid is incompressible, then it is its mass times the acceleration. If not, the fluid is compressible and we have to compute the waves propagating in the tubing, as has been implemented in the computational model (See Appendix D). The pressure P_{visc} was as calculated above and depends on the pump velocity.

This is the pressure the pump must overcome to move a viscous fluid in the tubing. This pressure is automatically computed in the computational model.

3.4.2 Pressure at the pump inlet in the well

The intake of the pump is located at its lowest point (see Figure 1-2)and pumps fluid located between the tubing and the casing. This fluid is provided by the reservoir, and reservoir modeling is beyond the scope of this research. An accurate reservoir model will output the fluid volume flow in the well and the fluid casing level can be computed. The casing is pressurized by the operator, and there is a fluid column $l_{fluid-casing}$ in the casing. Thus we have:

$$P_{intake} = P_{casing} + \rho_f g l_{fluid-casing}(t) \tag{3.10}$$

3.4.3 Pressure in the barrel below the plunger

The pressure in the barrel is the pressure below the plunger, $P_{plunger-}$. This pressure is key in understanding the functionality of the ball valves and varies throughout the stroke. We detail below how this pressure changes on the upstroke and the downstroke in the ideal case with no gas.

Upstroke

On the upstroke the standing valve is opened and the traveling valve is closed. Fluid is sucked in the barrel and a pressure drop occurs across the standing valve. The pressure drop across the valve is equal to the product of the fluid density, a valve constant K_v (dependent on the valve geometry) and the fluid velocity squared. The fluid velocity can be determined from the law of conservation of mass in the pump and the various cross sectional areas in the plunger and the ball valve.

$$
\begin{aligned}
P^{up}_{plunger-}(t) &= P_{intake} - P_{valve} \\
&= P_{casing} + \rho_f g l_{fluid} - \rho K_v \left(\frac{A_{plunger} \dot{\xi}(l,t)}{A_{valve}} \right)^2
\end{aligned}
\tag{3.11}
$$

Downstroke

On the downstroke the standing valve is closed and the traveling valve is opened. Fluid is pushed out of the barrel in the tubing above the pump, a pressure drop occurs across the traveling valve so the pressure below the plunger is higher than above.

$$
\begin{aligned}
P^{down}_{plunger-}(t) &= P_{plunger+} + P_{valve} \\
&= P_{plunger+} + \rho K_v \left(\frac{A_{plunger} \dot{\xi}(l,t)}{A_{valve}} \right)^2
\end{aligned}
\tag{3.12}
$$

Compression and Expansion events with valves closed

At the beginning of the upstroke and the end of the downstroke, both traveling and standing valves create a sealed (if we ignore fluid leakage) barrel volume. The barrel can contain either pure fluid, or a mixture of fluid and gas. If the well is empty or if it produces a lot of gas the barrel will ingest gas. We describe in the following the various situations corresponding to pure liquid phase or to a liquid and gas mixture in the barrel.

Pure liquid phase in the barrel

In this scenario the pump only sucks in liquid: this is the case if there is enough fluid in the casing above the pump. When both valves are closed (cf valve section), the plunger is either compressing or expanding the content in the barrel cavity. The pressure in the barrel depends on its relative change of volume and the fluid compressibility index β. The relative change of volume itself depends on the volume of the barrel cavity when the last ball valve closed $\mathcal{V}_{barrel}(t_{close})$ and the current barrel

volume $\mathcal{V}_{barrel}(t)$ at the time t. We can then compute the instantaneous pressure $P_{plunger-}(t)$ at the time t from:

$$P_{plunger-}(t) = P_{plunger-}(t_{close}) - \frac{1}{\beta}\frac{\mathcal{V}_{barrel}(t) - \mathcal{V}_{barrel}(t_{close})}{\mathcal{V}_{barrel}(t_{close})} \tag{3.13}$$

Liquid and gas mixture in the barrel

If the liquid level in the casing is too low, a mixture of liquid and gas will be sucked into the pump barrel. In that case the fluid in the barrel is taken to be incompressible and only the gas is compressible. This was verified by using real gas table properties at 3000m depth and the gas was found to be orders of magnitude more compressible than the liquid.

We calculate the Fourier number $F_0 = \frac{\alpha_t t}{L^2}$ to determine if the compression/ expansion will be isothermal or isentropic. α_t is the thermal diffusivity of the barrel metal, t is the compression time (typically 1-2 seconds) and L is the barrel thickness. At Fourier number higher than 1 the thermal diffusion is significant and there is a thermal equilibrium between the inside and outside of the pump barrel. For low Fourier number the content of the barrel is considered to be thermally insulated from the outside.

We find $F_0 << 1$ so the gas is assumed to be compressed isentropically and PV^γ =constant.

Numerically the barrel volume is computed at every time step and the corresponding barrel pressure is evaluated. Depending upon the barrel pressure the valves open or closed state is then evaluated.

3.4.4 Viscous Fluid Shear and Flow Leakage at the Plunger

Viscous Fluid Shear

The barrel and the plunger are designed so that a thin gap exists between the two components in relative motion for lubrication purposes, with the plunger moving relative to the barrel. Fluid is allowed to flow in a small gap between the plunger and barrel. This helps to lubricate the pump and to improve its reliability over time. The pressure above the plunger is equal to the hydrostatic pressure in the tubing, while the pressure below the plunger in the barrel changes during the stroke.

The flow in the gap can usefully be viewed as a superposition of two familiar characteristic flows: one a Couette flow driven by the shear force of the wall acting on a viscous liquid, and the other a Poiseuille flow driven by a pressure difference between two ends of a fluid.

Since the gap e is small in front of the plunger radius $e << R_{plunger}$, we can analyze the flow in the gap in a cartesian geometry and neglect the radius of curvature.

Using the thin film theory we find, with ΔP_{pump} the difference of pressure across the pump, e the gap between the plunger and the barrel wall, $L_{plunger}$ the plunger length and $V_{plunger} = \dot{\xi}(l,t)$ the plunger velocity, that:

$$F_{visc} = \pi R_{plunger} e \Delta P_{pump} - 2\pi R_{plunger} L_{plunger} \mu \frac{V_{plunger}}{e} \tag{3.14}$$

This is the force applied on the plunger. The fluid velocity profile around the plunger is illustrated in Figure 3-6, the flow in the gap on the upstroke is illustrated on the left while the downstroke flow is illustrated on the right.

The expression of the ratio of the force induced by the Poiseuille flow, $\pi R_{plunger} e \Delta P_{pump}$, to that induced by the Couette flow, $2\pi R_{plunger} L_{plunger} \mu \frac{V_{plunger}}{e}$, can be rearranged so that it is a product of a local Reynolds number $\frac{e \rho_f V_{plunger}}{\mu}$, a geometric parameter $\frac{e}{2L_{plunger}}$ and a non-dimensionalised pressure coefficient $\frac{\Delta P}{\rho_f V_{plunger}^2}$ i.e. :

$$\frac{F_{viscPoiseuille}}{F_{viscCouette}} = \left(\frac{\Delta P}{\rho_f V_{plunger}^2}\right)\left(\frac{e}{2L_{plunger}}\right)\left(\frac{e \rho_f V_{plunger}}{\mu}\right) \tag{3.15}$$

During the upstroke the "Poiseuille force" dominates ($\frac{F_{viscPoiseuille}}{F_{viscCouette}} >> 1$) and during the downstroke they are both of similar magnitudes ($\frac{F_{viscPoiseuille}}{F_{viscCouette}} \approx 1$).

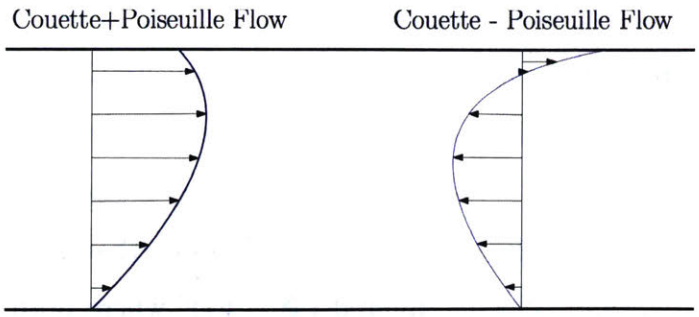

Figure 3-6: Representative velocity profiles in the gap between plunger and barrel.

Flow Leakage at the Plunger

The leakage flow is significant on the upstroke when the pressure difference ΔP_{pump} across the plunger is maximum. During the downstroke the barrel pressure increases thus reducing the pressure differential across the plunger and reducing the leakage flow. We will elucidate how the this flow is critical in allowing the fluid to exit the gas lock operating mode.

3.5 Wave Equation and Damping Evaluation

3.5.1 Wave Equation

The wave equation describing the dynamics of the rod system is:

$$\frac{\partial^2 \xi}{\partial t^2}(x,t) = c^2 \frac{\partial^2 \xi}{\partial x^2}(x,t) + \lambda \frac{\partial \xi}{\partial t}(x,t) + \Lambda(\frac{\partial \xi}{\partial t}(x,t) - V_f(x,t))^2 + g \tag{3.16}$$

The wave equation we are solving contains three key parameters:

- the damping λ at the rod-fluid interface
- the sound velocity c in the rod
- the non-linear fluid-structure coupling Λ that depends on the local relative velocity between the fluid and the rod $\frac{\partial \xi}{\partial t}(x,t) - V_f(x,t)$

The subject on rod-fluid coupling will be further elaborated in the following chapter where we will show that the couplers/centralizers along the rod cause a pressure drop. This pressure drop applies a force at every coupler that can be assumed to be continuous since the spacing between couplers is small compare to the wavelengths of the waves propagating along the rod. We will show that this force scales with the local relative rod-fluid velocity squared $(\frac{\partial \xi}{\partial t} - V_f)^2$ where both ξ and V_f have a functional dependence on (x,t). This creates a non-linear damping.

3.5.2 Rod Damping

Upstroke λ^{up} and downstroke λ^{down} viscous distributed damping

The viscous rod damping coefficient λ varies temporally and spatially along the rod. However as a first approach it is useful to assume it to be time invariant and uniform along the rod string during each up/downstroke phase. We will next detail the calculation for the upstroke phase λ^{up}.

The upstroke distributed damping λ^{up} is created by a superposition of several sources of damping. First the bulk flow creates a shear force on the rod, then the rod oscillates at its natural frequency while moving, creating an additional damping.

The rod does not have a uniform velocity. As such the velocity profile in the vicinity of the rod surface will deviate by $\delta v(x, r, t)$ from the bulk velocity profile V.

$$v(x, r, t) = V(r, t) + \delta v(x, r, t) \tag{3.17}$$

This δv can be estimated using the solution to Stokes second problem. To do so we need to known how the rod is oscillating at its natural frequency with an amplitude A_n.

To calculate the amplitude of the rod oscillations, we evaluate the maximum response of a mass spring system to a constant velocity displacement. The motion of the polished rod at the surface is assumed to be of constant velocity during a stroke, with different velocity on the upstroke and downstroke.

The system is initially at rest. $\xi(l, t)$ is the pump position, $\xi(0, t)$ is the polished

rod position (top of the spring) as seen in Figure 3-7. The response of that system is illustrated in Figure 3-8 and is elaborated below. c_{damp} is the viscous damping coefficient such that the force applied to the mass, at the end of the rod string, is $c_{damp}\frac{\partial\xi(l,t)}{\partial t}$, and is linked to λ^{up} by geometric coefficients set by the geometry property of system(cf Appendix). We assume $c_{damp} << 1$ to obtain an upper value of the amplitude A_n. This assumption can be verified once we evaluate λ^{up} by comparing it to c_{damp}.

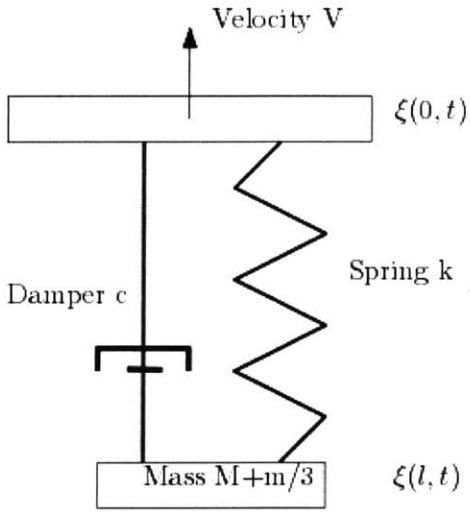

Figure 3-7: One degree of freedom Oscillator

We know that for a system initially at rest the mass (i.e. the pump in our case) position will be the convolution of the forcing function $\xi(0,t)$ and the impulse response function for absolute displacement by virtue of absolute ground displacement $h_{\xi(l,t)|\xi(0,t)}$. In our case the ground reference is the polished rod (name of the rod at the top) and its position over time is $\xi(0,t) = Vt$ and $\xi(l,t)$ is the pump position. the polished rod is here assumed to have a constant velocity. This is usually a valid approximation since the pump only starts moving once the rod has stretched enough and has an almost constant velocity.

$$\xi(l,t) = \xi(0,t) * h_{\xi(l,t)|\xi(0,t)} \tag{3.18}$$

We obtain the pump position as a function of the imposed velocity V, natural pulsation ω_n, rod mass m, lifted mass M, and system damping c_{damp}:

$$\xi(l,t) = Vt - \frac{V}{\omega_n} exp^{-\frac{c_{damp}}{2(m/3+M)}} sin(\omega_n t) \tag{3.19}$$

The pump response is shown in Figure 3-8. The pump and the polished rod do not start simultaneously as the rod initially stretches building up a load equal to the fluid weight. The pump initially jerks upwards at a velocity higher than the top of the rod and then oscillates at the fundamental resonance frequency.

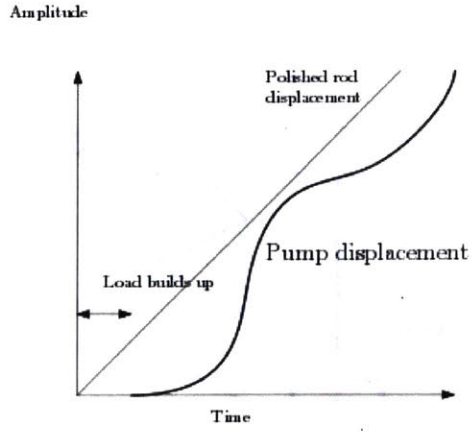

Figure 3-8: One degree of freedom oscillator response to a constant velocity input

We find the solution to Stokes second problem, assuming we have a planar semi infinite geometry (no outer tubing wall), where each rod section has a phase difference in position ϕ with the top of the rod (i.e. every section of rod oscillates at the same frequency and amplitude but they are out of phase since compression waves are traveling along the rod) as:

$$v(x,r,t) = A_n cos(\omega_n t - (r - R_{rod})/\delta + \phi(x)) e^{-\frac{(r-R_{rod})}{\delta}} \tag{3.20}$$

This velocity profile is illustrated in Figure 3-9 and the thickness of the oscillating boundary δ is expressed below, with ν the kinematic viscosity.

$$\delta = \sqrt{\frac{2\nu}{\omega_n}} \tag{3.21}$$

We have now calculated the two velocity components of $v(x,r,t) = V(r,t) + \delta v(x,r,t)$. The next step is to evaluated the fluid shear force applied on the rod.

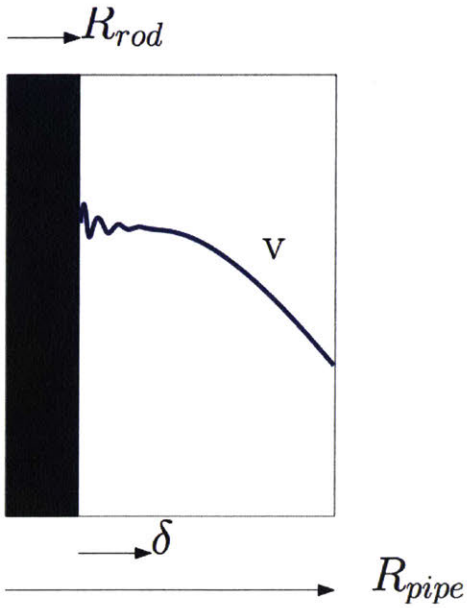

Figure 3-9: A sketch illustrating a representative velocity profile across a pipe cross section; delta is the region within which oscillatory velocity component due to wave motion along the rod is finite

The shear forces applied on the rod can be decomposed into two components:

- A shear force that depends on the bulk motion of the flow $\bar{V}(r)$
- A local shear force that depends on the local rod vibrational frequency and amplitude

Knowing the previously calculated velocity profile, we can compute the viscous shear forces on the rod and this yields the damping coefficient λ^{up}. The exact same strategy for the solution as for the upstroke is used for the downstroke to evaluate λ^{down}.

3.5.3 Rod Boundaries

To solve the wave equation, we need to understand how the rod is attached at the surface and at the bottom, mathematically this means formulating the boundaries conditions of the system.

The top boundary condition is set by the rod imposed movement and is of Dirichlet type. The top of the rod (the polished rod) is attached to the horsehead which is

itself connected to a motor through various linkages and gears. The compliance of the top driving unit will be neglected as a well designed structure should be stiff compare to the rod.

Since the polished rod is attached via cables to the horsehead, no compressive load can be transmitted. This is usually a non issues since the rod assembly and the pump are heavy enough to maintain the system under tensile load at the top at all time.

The attributes of the bottom boundary dictate the adequacy of the model. Many off designs conditions are created by phenomena occurring at the bottom of the well such as the presence of gas due to the lack of fluid to pump. A full force balance is done on the pump and the pump can be modeled as a piston moving in a pipe.

The forces acting on the pump are delineated below:

- the pump weight
- the rod tension/compression
- the pressure above/below the pump
- the shear force applied on the side of the pump by the leaking (by design) lubricating fluid

3.6 Analytical Solution

We can simplify the rod-pump system further to obtain a relatively simple solution that would allow one to grasp the essence of the problem and the key non dimensional controlling parameters. The rod can be modeled as a transmission line terminated by a complex impedance, the downhole pump. There is no non-linear rod-fluid coupling here. This approach is possible as long as all the system parameters are constant throughout a stroke (i.e upstroke and downstroke parameters are identical). The fluid is taken to be incompressible and viscous.

The analytical solution provides insights into the key functionalities of the system but it can not be used to provide quantitative results. The solution cannot be used

in situations where non-linear effects such as those associated with the operation of the opening and closing of one way valves used in the pump. This is why the analytical model was mainly used as a benchmark to assess the accuracy of the numerical implementation of the model, as detailed in Appendix B.

The plunger area is assumed to be equal to the tubing area. The lifted mass is the sum of the fluid mass, one third of the rod mass and the pump mass. The lifted mass is taken to be identical for both the up and downstroke; the upstroke pump damping coefficient λ_{up} is used for both the up and the downstroke.

The analytical solution of the wave equation A.2 for a single pulsation ω ($\omega = 2\pi f$) assumes the form given in equation 3.22.

$$\xi(x,t) = \mathcal{A}_{top} f(x) e^{i\omega t} \tag{3.22}$$

The funtion f(x) is determined from the two imposed boundary conditions, the imposed motion at the top and the dynamic response set by the force balance at the bottom.

From the wave equation A.2 we obtain:

$$f(x) = Acos(kx) + Bsin(kx) \tag{3.23}$$

To find the constants A and B we use the boundary equations presented in the following.

At the top:

$$\xi(0,t) = \mathcal{A}_{top} e^{i\omega t} \tag{3.24}$$

We obtain f(0)=1.

At the bottom the pump is assumed to have a fixed mass m_{pump} and a fixed damping coefficient Z_R.

$$m\frac{\partial^2\xi^*}{\partial t^2}(l,t) = -EA_{rod}\frac{\partial\xi^*}{\partial x}(l,t) + Z_R\frac{\partial\xi^*}{\partial t}(l,t) \tag{3.25}$$

The complex impedance of the system is given as:

$$Z = Z_R + i\omega m \tag{3.26}$$

The rod has its own impedance, and for no damping, it can be approximated as:

$$Z_{rod} = \frac{EAk^{wave}}{\omega} \approx \rho c A_{rod} \tag{3.27}$$

With Z as the pump impedance, and with $\omega = \frac{2\pi}{T}$, we have:

$$f(x) = cos(k^{wave}x) - \frac{j\frac{Z}{Z_{rod}}cotan(k^{wave}l) - 1}{j\frac{Z}{Z_{rod}} + cotan(k^{wave}l)}sin(k^{wave}x) \tag{3.28}$$

The solution is, after normalizing the result by the driving amplitude $\mathcal{A}_{top}$:

$$\frac{\xi(x,t)}{\mathcal{A}_{top}} = \left(cos(k^{wave}x) - \frac{j\frac{Z}{Z_{rod}}cotan(k^{wave}l) - 1}{j\frac{Z}{Z_{rod}} + cotan(k^{wave}l)}sin(kx)\right)cos(\omega t) \tag{3.29}$$

Z is the pump impedance that depends on the damping and the lifted mass, Z_{rod} is the rod impedance that depends on its radius and material properties, k is the wave number. The wave number k has a real part k_r^{wave} that corresponds to the wave propagation characteristic and an imaginary part k_i^{wave} that is the source of the wave amplitude attenuation (damping or absorption) along the rod. We find k^{wave} from a dispersion relation obtained by substituting the solution into the wave equation.

An example result is shown in Figure 3-10, and the pump amplitude is visible based on the imposed sinusoidal imposed motion at the top on the polished rod.

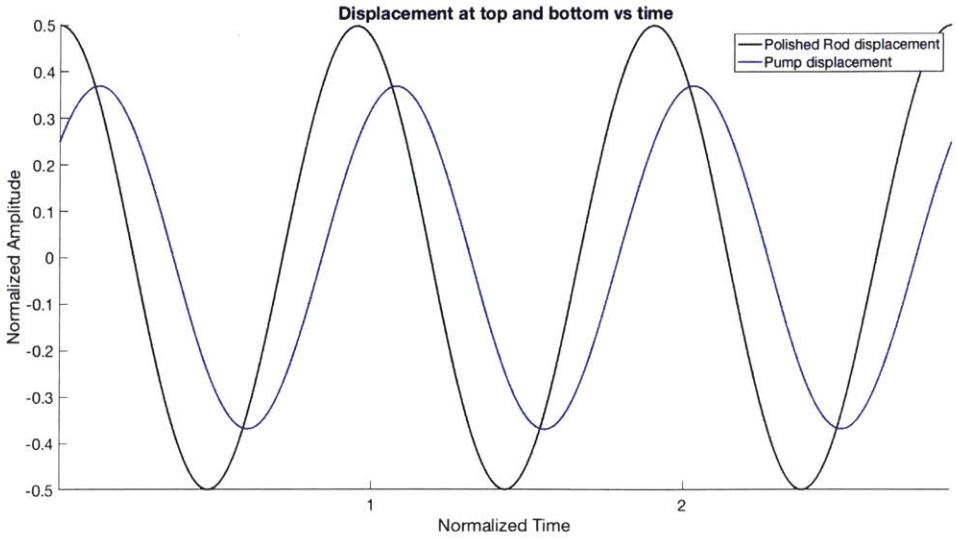

Figure 3-10: Pump amplitude as calculated using the analytical model for a 1000m well lifting 5 metric tons of fluid

3.7 Computational Model

There are many situations where it is useful to seek a numerical solution to the equations governing the rod pump system operation as they do not always have an analytical solution. A numerical solution can almost always be obtained effectively for the problem formulated here.

To numerically solve a PDE, a time and a space grid are created. As it is to be expected, the solution accuracy depends on the grid resolution. The scheme is detailed in Appendix D. Since the range of frequencies typically encountered is both small and low (0.1Hz to 5Hz) compare to the numerical model time steps (khz), dispersion is not critical and a scheme preserving amplitude was selected.

3.8 Parametric Study

The following parametric study was done on Sandia well 1 and since the analysis has been implemented based on non-dimensional basis the results should be applicable to any well.

3.8.1 Rod stiffness effect

We start by looking at the effect of the rod stiffness. This was done by changing the young modulus of the rod which has many effects. In the wave equation, $\Pi_5 = \sqrt{\frac{E}{\rho}}\frac{T}{l} = \frac{cT}{l}$ is modified. The stiffer the rod the higher the natural frequency would be, and this is why we observe more high frequency noise at higher stiffnesses on both the surface and the pump cards. But more importantly we see many more oscillations on the surface card at higher rod stiffnesses. The higher the system natural frequency is, the more oscillations will be visible in a given timeframe such as upstroke or downstroke.

Increasing the rod stiffness also alters $\Pi_7 = \frac{m_{fluid}g}{k\mathcal{A}_{top}}$, $\Pi_8 = \frac{m_{pump}}{kT^2}$ and $\Pi_9 = \frac{Z_R}{kT}$. As we increase k, the rod stretch due to the fluid weight decreases (stiffer spring to pick up a given mass) and Π_7 drops, thus the pump amplitude also increases and converges towards $\mathcal{A}_{top}$, the polished rod amplitude. The pump impedance, with the reactance taken into account in Π_8 and the resistance in Π_9 decreases with a stiffer rod. Thus there is less damping with vibrations of larger amplitude. This effect is exacerbated by the higher reduced frequency in the rod as more waves now travel up and down the rod simultaneously. The consequence is a relatively more noisy pump card.

On the surface card we also observe that the initial slope of stress vs position increases with the rod stiffness, this is expected since that slope is the rod stiffness.

In a quasi-steady system, the rod behaves like a spring and the rod stretch under load is equal to the load over the rod stiffness. As expected, since most wells are acoustically compact in the rod, we find that the stretch varies as 1/rod stiffness.

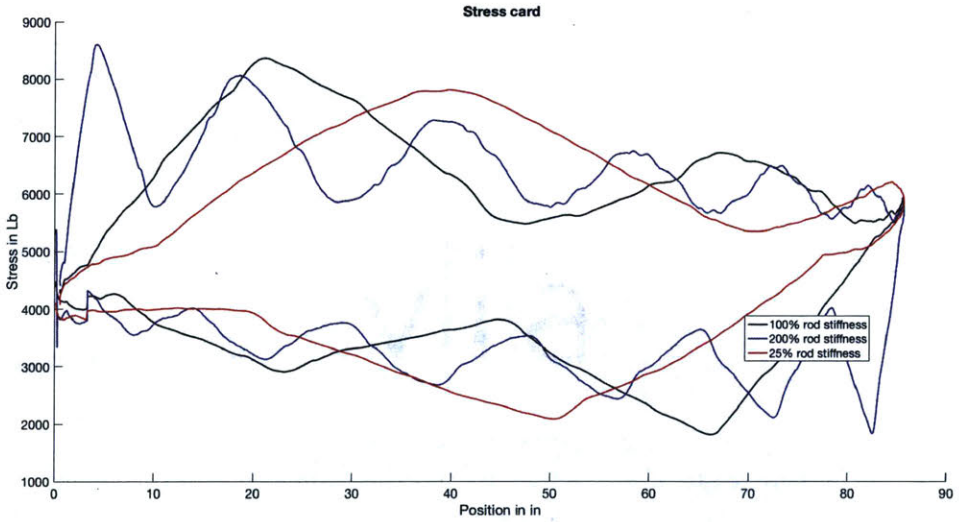

Figure 3-11: Rod stiffness effect on the surface card.

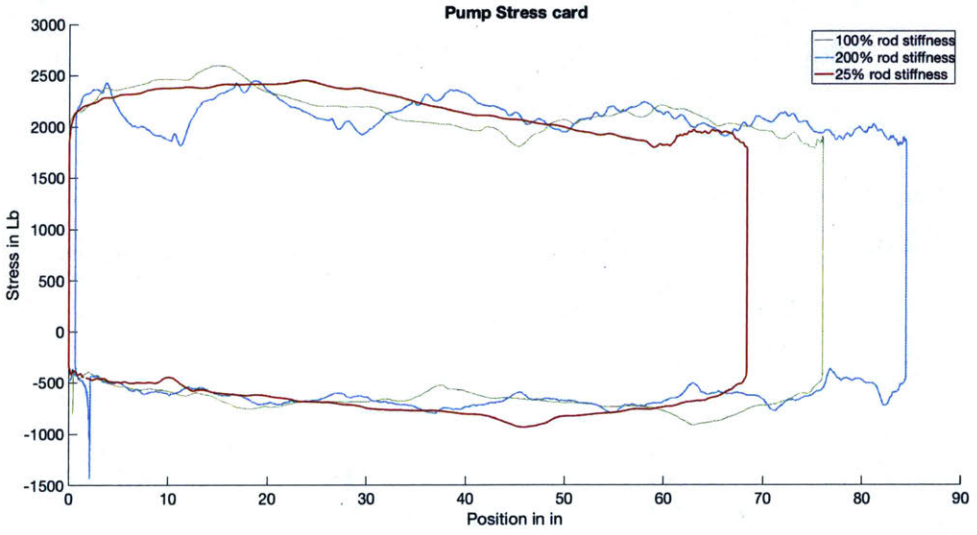

Figure 3-12: Rod stiffness effect on the Pump card

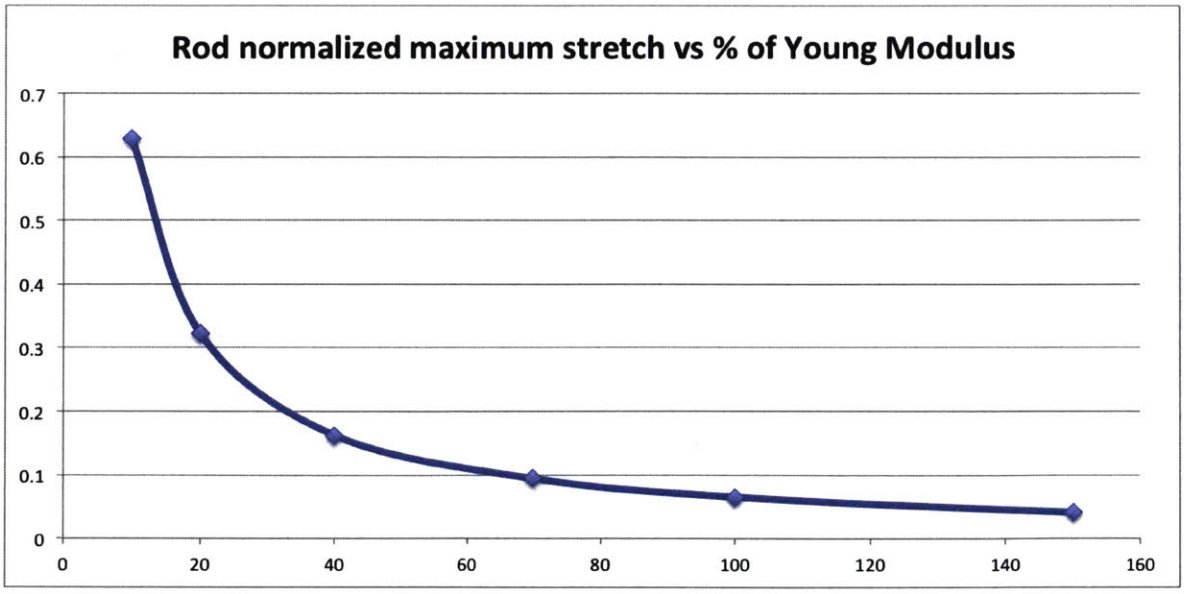

Figure 3-13: Normalized stretch vs Young Modulus %

3.8.2 Driving frequency effect

Changing the pumpjack motor gearing will change the main driving frequency, which will alter Π_5,Π_8 and Π_9.

We observe two key effects in the surface card:

- the number of visible oscillations during a stroke increases as the driving period increases. Simply put the system has more time to oscillate at its natural frequency during the upstroke/downstroke.

- the amplitudes of stress oscillations varies greatly. At very large driving periods, Π_8 and Π_9 converge towards 0 and the system becomes quasi-steady. In contrast, at low driving periods the system is highly dynamic and the effects created by the pump start to dominate the movement.

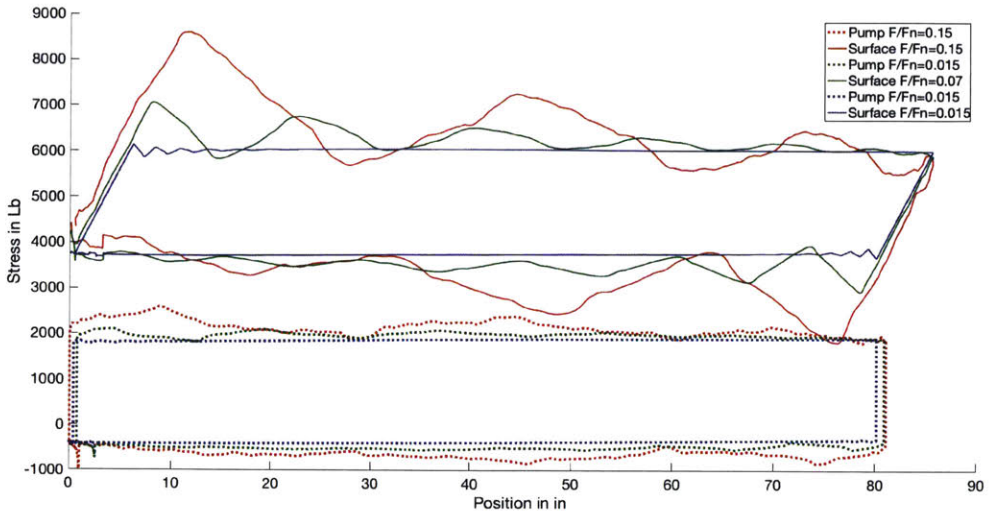

Figure 3-14: Driving frequency effect on the surface card, as a function of the driving frequency of the system natural frequency

3.8.3 Driving amplitude effect

The results from rod damping analysis show that, at lower amplitude, the system velocities are lower thus the dynamic responses of the system, especially the maximum stress reached on the surface card, are lower. In addition, the smaller the amplitude; the larger the rod stretch is relative to that amplitude, this effect is captured in the number $\Pi_7 = \frac{m_{fluid}g}{k\mathcal{A}_{top}}$. This means that as long as the rod stress is within the safe limits, the amplitude should be as high as possible.

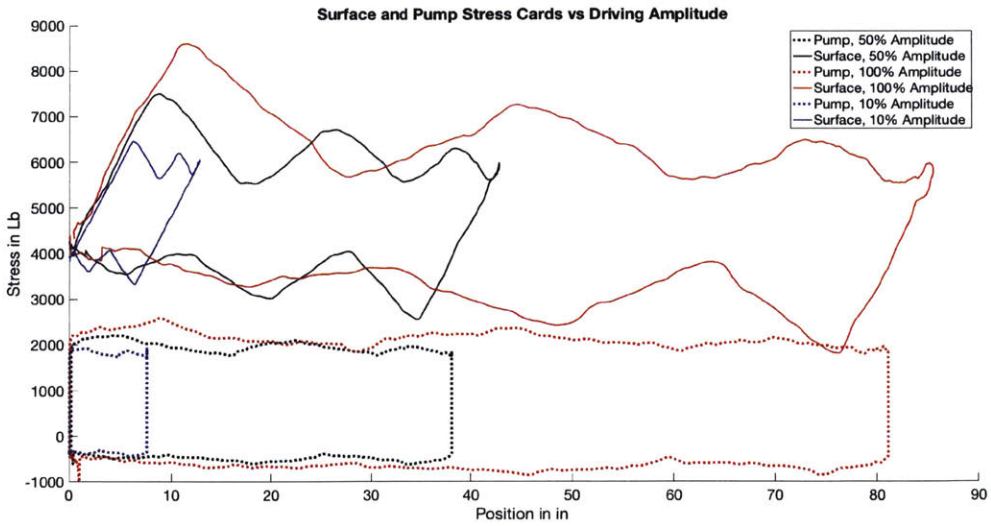

Figure 3-15: Driving Amplitude effect on the surface card

3.9 Summary

The attributes of a rod-pump system model are formulated in this chapter. The key time scales characterizing the pump operations have been identified and quantified. These various time scales are useful in the interpretation of the measured pump charts. The fluid velocity profiles have been determined; the determined fluid velocity profiles enable one to evaluate the damping created by the fluid-structure interaction along the rod. With the damping quantified, the equations governing the rod dynamics can next be solved using a temporal and spatial discretization scheme. A closed-form analytical solution was obtained with further simplifying assumptions; this analytical solution enables one to get at the essence of the pump dynamics and the characterizing non-dimensional parameters useful for establishing the scaling.

Chapter 4

System Acoustic Model and Scaling

4.1 Introduction

In this chapter, the assumption that the fluid is incompressible will be relaxed. This means that we will obtain a coupled system that consist of two compressible mediums: the rod string and the column of fluid.

The fluid column will be mathematically modeled using the equations previously developed, and will be coupled to the rod string at the bottom boundary to the pump.

4.2 Acoustic Wave Equation

4.2.1 Simplifying Assumptions

Previous research work [12] has shown that the flow can not be assumed to be incompressible for wells with reduced frequency $cT/l \approx 1$ (most existing wells fall into this category). This is especially true if we wish to use the pressure signal to diagnose issues associated with high frequencies such as valve opening or closing. We will make several assumptions in order to simplify the model. They are of minor impact and can be relaxed when needed to. The fluid is assumed to be isothermal and the phys-

ical properties of the fluid are assumed to be independent of pressure. The physical properties do not depend on the depth or the position along the rod. The fluid is assumed to be homogenous and single phase, i.e. the presence of gas affects the bulk properties of the fluid only.

These simplifying assumptions lead to the need of only three quantities to define the fluid physical properties:

Density ρ

Viscosity μ

Isothermal Compressibility β

From these we can determine the fluid sound velocity c_f.

The acoustic pressure can be estimated by the fluid impedance times the pump velocity, which gives us an acoustic pressure in the order of a couple atmospheres. Since that pressure is orders of magnitudes lower than the hydrostatic pressure found in a well except very close to the surface, it's effect on the tubing radial stretch is negligible. In addition the hoop stress analysis was done on the tubing and the radial stretch was found to be of no importance for the systems that have been assessed and examined.

4.2.2 Fluid wave equation

Below is the full fluid pressure wave equation that is solved in parallel with the rod wave equation. The various terms and boundary conditions necessary to solve it are detailed in the following sections.

$$\frac{\partial^2 P}{\partial t^2} = c_f^2 \frac{\partial^2 P}{\partial x^2} + \lambda_P \frac{\partial P}{\partial t} + \frac{4\nu}{3} \frac{\partial P^3}{\partial t \partial x^2} + \Lambda_P \frac{\partial (v_{fluid}(x,t) - v_{rod}(x,t))^2}{\partial x} \tag{4.1}$$

As with the rod wave equation, we start with the standard pressure wave equation $\frac{\partial^2 P}{\partial t^2} = c_f^2 \frac{\partial^2 P}{\partial x^2}$ with c_f the sound velocity in the fluid. The following three terms are damping terms, each corresponding to a different physical phenomenon.

- The first damping term with the damping coefficient λ_P corresponds to the viscous losses between the fluid and the tubing/rod interfaces. This damping affects the amplitude of the pressure waves.

- The second damping term with the damping coefficient $\frac{4\nu}{3}$ is due to the fluid inherent viscosity. This term becomes critical for frequencies in the kHz range in water (sonar applications). It also scales with the fluid viscosity so the term can also be important at low frequencies if the waves are propagating in heavy crude oil. In our application we assume the fluid is water so this term becomes negligible. This term acts as a low pass filter.

- The last damping term with the damping coefficient Λ_P is created by the interaction between the fluid and the moving obstacles such as centralisers and couplers along the rod. It is a non linear term that depends on the relative velocity between the fluid and the rod. The term Λ_P primarily scales with the area ratio before and after an obstacle on the flow path, the number of obstacles and the distance between the obstacles.

4.2.3 Top Boundary

A one way adjustable backpressure check valve is placed at the top of the tubing. If the fluid has a higher pressure than a set pressure, the valve opens and the well can flow. If the pressure is lower than the set pressure then the valve acts as a solid wall. When the valve is open it is assumed that there is no reflection coming from the end of that pipe.

In mathematical terms we obtain a Neumann boundary condition if P(0,t) (where we have used P(x,t) to denote the fluid pressure at the position x and time t) is below the set pressure, with 0 velocity. If P(0,t) is above the set pressure then we

have a non-reflecting Sommerfeld radiative boundary. Numerically this is done by discretizing the first order wave equation, the advection equation, in the negative x direction (from the bottom to the surface) below:

$$\frac{\partial P}{\partial t} - c_f \frac{\partial P}{\partial x} = 0 \tag{4.2}$$

By enforcing equation 4.2 at the boundary, waves can only leave the computational domain and are not reflected.

The current valve model is approximate as a real check valve progressively opens between its set cracking pressure and the full flow pressure at which the valve is fully open.

Physically a pressure sensor can be placed at the top of the well to measure surface pressure, and one could conceive a system where additional sensors are used (as long as they are separated by a couple wavelengths to provide useful different information). One useful application for this would be placing a sensor at a critical depth that is calculated so that the gas in the pumped liquid is dissolved, since it can come out of solution close to the well surface.

4.2.4 Bottom Boundary

The rod dynamics are primarily coupled to the fluid dynamics via the pump (the rod last segment). The pump creates acoustic waves at the bottom of the well: these waves then travel in the tubing before being reflected at the surface causing a fluid-structure coupling.

Waves in the fluid can alter the pump position which then causes stress waves in the rod. We consider the following three cases. The first two are approximations that are easy to implement and allow an analytical solution while the third case is a situation where one needs to use a numerical solution.

Incompressible Flow

$$\frac{l}{c_f T} << 1 \tag{4.3}$$

To begin with it is useful to consider the fluid as incompressible, i.e. acoustic wavelengths are much longer than the well length. Numerically we applied a force equal to a mass times the plunger acceleration. The dynamic pressure is thus equal to:

$$P_{dynamic} = \rho l \ddot{\xi}(l,t) \tag{4.4}$$

Infinite propagation

$$\frac{l}{c_f T} >> 1 \tag{4.5}$$

The opposite approach is to consider the fluid as compressible but the well as infinitely long, i.e there are acoustic waves generated by the pump but they are not reflected at the surface. Physically this occur when the well is long. The waves generated at the pump are attenuated and have a negligible amplitude by the time they have travelled from the bottom to the top,and are reflected back to the bottom of the well.
The pump radiates pressure waves in the fluid, the pressure is by definition equal to the fluid impedance per unit area $Z_R/A_{plunger} = \rho c_f$ times the plunger velocity and area. The dynamic pressure (defined in the previous chapter as the pressure at the pump minus the hydrostatic pressure) is thus equal to:

$$P_{dynamic} = \rho c_f \dot{\xi}(l,t) \tag{4.6}$$

Fully coupled model

The fluid compressibility is taken into account to describe the acoustic waves in the system. Typically short wells have a large coupling between the fluid pressure waves and the rod dynamics as the pressure waves are not damped as much as in longer wells. Increasing the pump plungers size also increase rod-fluid coupling because of the increased pressure force applied as the force increases linearly with the area. In order to numerically solve that fluid structure interaction, we match the acceleration and velocity of the last fluid section, in front of the pump, with the pump. This is done in an Lagrangian approach in order to follow the pump plunger.

- The rod position is evaluated at time step i+1 using forces at the time i
- The new rod acceleration at time step i+1 is evaluated
- the pressure field at time step i is interpolated onto the rod position at time step i+1
- the interpolated pressure field at time step i is used to compute the pressure field at i+1 except at the last point, the pump
- the pressure field at the last point at i+1 is evaluated using Euler equation below

Euler equation links the spatial pressure gradient in the fluid to its density and its material derivative.

$$\rho_f(\frac{\partial V_f}{\partial t} + V_f \nabla V_f) = -\frac{\partial P_{dynamic}}{\partial x} \tag{4.7}$$

This boundary condition holds for any well and links the pressure force on the piston to the fluid velocity.

4.3 Propagation of Pressure Waves

Just like the stress waves in the rod, we have longitudinal compressive waves in the fluid. Since we are interested in frequencies <100Hz, we are looking at wavelengths of 15m or more for a representative well. We can assume the waves to be one-dimensional since the pipe diameter R_p (about 10cm) is several order of magnitudes smaller than the wave lengths. Both the effect of pipe curvature and pipe elasticity have been assessed and are presented in Appendix C. Pipe curvature effect is negligible in our frequency range while pipe elasticity can alter the acoustic velocity by about 5% for a steel pipe. Considering the range of reduced frequencies encountered, there are both acoustic as well as hydrostatic effects that modulate the surface pressure.

4.3.1 Distributed Fluid-Structure Coupling

The rod string is not of uniform diameter. At every rod joint (about every 9m) there is a coupler (female-female threaded joint) which has a larger diameter than the rod. In addition to the rod couplers, centralizers are usually used in deviated section of the well with 2-4 centralizers per rod. This means that an average well can have several hundreds of obstacles on the flow path. We assume here couplers and centralizers have the same cross sectional area.

On the upstroke the fluid and the rod both move upwards at a similar velocity. On the downstroke they move in opposite direction with a large relative velocity difference thus creating a significant pressure drop at each obstacle. This was modeled as a sudden contraction and sudden expansion. We find that the pressure drop $\Delta P_{coupler}$ across a coupler depends on the coupler area $A_{coupler}$, the tubing area A_{tubing}, the rod area A_{rod}. Those parameters are lumped into the coefficient C_3. The local fluid relative velocity $v_{rel}(x,t) = v_{fluid}(x,t) - v_{rod}(x,t)$ is key in evaluating the coupling and is the source of the non linear damping.

$$\Delta P_{coupler}(x,t) = C_3 \rho_f v_{rel}(x,t)^2 \tag{4.8}$$

The couplers are, at maximum, one rod length apart (about 9m) which is smaller than the wavelengths of interest; we can take the pressure drop to be continuous and average it over the length of the rod l. We obtain a pressure drop per unit length that depends on the total number of couplers $n_{couplers}$.

$$\frac{\partial P_{coupler}}{\partial x}(x,t) = \frac{n_{couplers}}{l} \Delta P_{coupler}(x,t) \tag{4.9}$$

Numerically this damping is more challenging to compute and requires to significantly higher code spatial and temporal resolution hence larger computational resources. We find this term to be important only in deviated wells that use a large number of centralizers.

4.3.2 Viscous Pressure damping

Since the fluid viscosity is not equal to zero, we can expect that the pressure waves will be partially attenuated as energy is dissipated into heat. This dissipation is taken into account by adding a term in the wave equation. For a fluid like water we can expect the damping to be weak at low frequencies; nevertheless this effect is incorporated into the model to add implementational flexibility and to allow the simulation of fluid with high oil percentage. Using Stokes wave equation we find that including the viscous effects adds a term in the wave equation that depends on the fluid kinematic viscosity: $\frac{4\nu}{3}\frac{\partial P^3}{\partial t \partial x^2}$

4.3.3 Pressure damping λ_P

This damping constant affects the amplitude of the signal. The amount of gas in the tubing is expected to be the key parameter for this damping, and while it is theoretically complicated to model the damping, it is straightforward to experimentally determine this constant. Since the signal analysis done here is focused on the pressure signal phase this damping is not an important parameter for the model and as such it was not assessed further.

4.4 Parametric Study

The following study was done on a 724m well running at 6.3 strokes per minute. This well has been fully instrumented specifically for this PhD research and is located in South Oklahoma.

4.4.1 Damping parameter

The linear damping parameters, which depends on the flow characteristics in the tubing, removes the high frequency content in the signal and decrease the amplitude of the signal as visualized in Figure 4-1. Experimentally it was noted that wells producing gas have a higher linear damping.

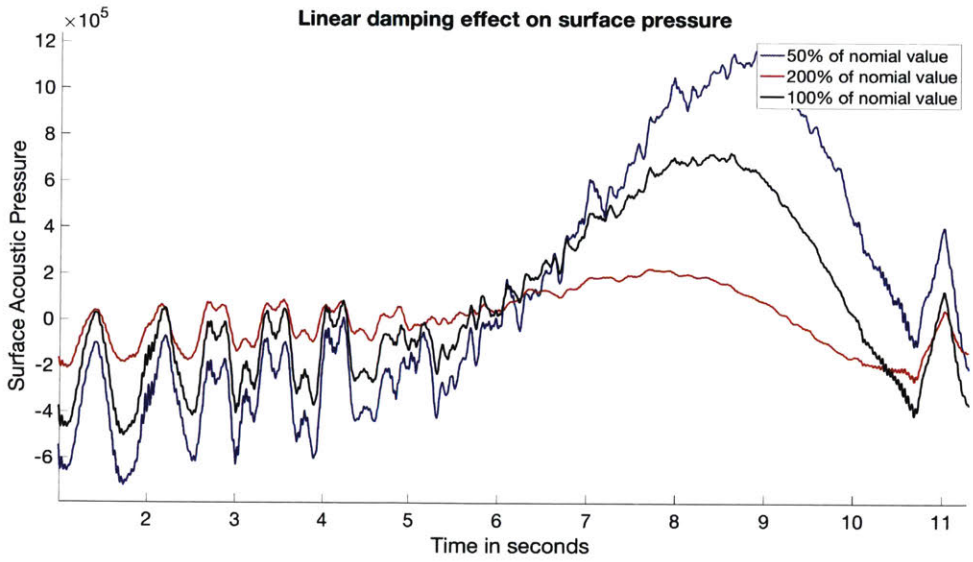

Figure 4-1: Effect of the linear damping on the computed surface signal. The signal amplitude is sensitive to that damping.

4.4.2 Rod tappering

The rod tapering effect can be critical in some wells where the change of rod cross-section is significant. Specifically, we study the effect of the polished rod in Figure 4-2. This is the first rod at the surface of the well and it is of much larger diameter than the rest of the rod string. In addition the change of cross section is very close (compare to a wavelength in the fluid) to the surface which increases its effect on the surface pressure.

On the downstroke the polished rod is pushed down and displaces fluid close to the surface which creates a positive pressure, this is visible as a large positive pressure oscillation. Similarly on the downstroke the rod is pulled out of the well and creates a negative pressure.

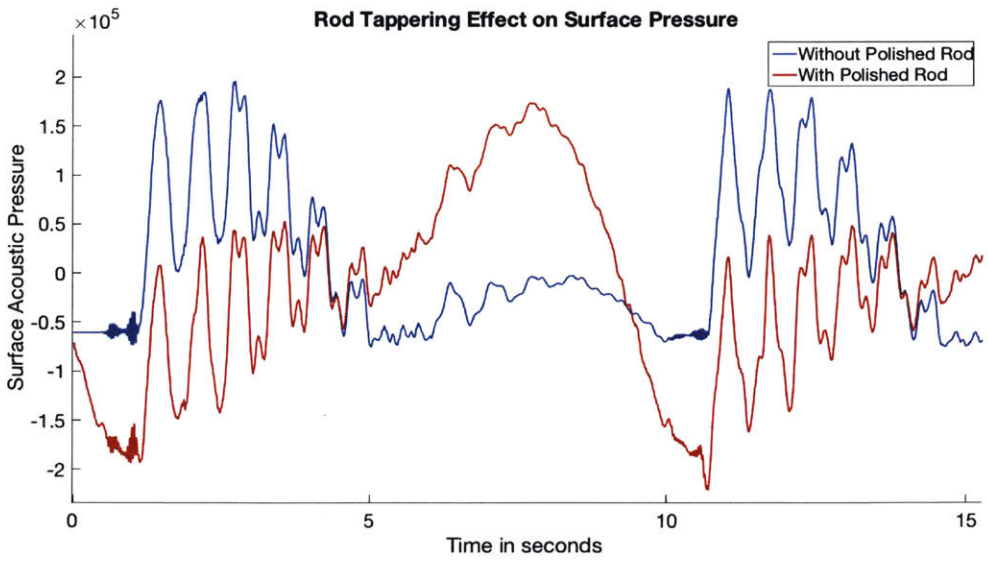

Figure 4-2: Effect of the polished rod on the computed surface signal. The polished rod is a sucker rod of much larger diameter (about 2X) than the typical rod and is attached right at the well surface.

4.4.3 Fluid Sound Velocity

Similarly to the study of waves in the rod, changing the sound velocities affect many non dimensional parameters related to the waves damping. As expected we also see a phase difference between the signal created by the additional time needed to propagate the signal.

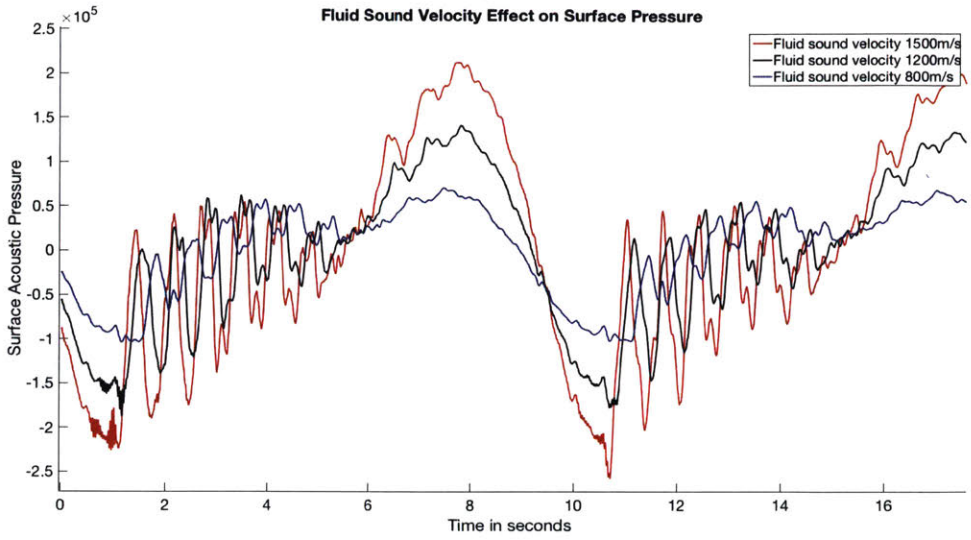

Figure 4-3: As the sound velocity drops the dynamic effects are damped out.

4.4.4 Surface boundary

We examine here three types of boundaries:

- Neumann boundary: this boundary reflects every waves and creates a lot of high frequency noise
- A Sommerfeld boundary that creates no reflection (semi-infinite pipe)
- A Robin mixed boundary, that act as a Sommerfeld boundary above a set pressure and as a Neumann boundary below it

It was found that the Sommerfeld boundary yield a result similar to the one obtained using the mixed boundary while being more computationally robust and was thus used for every simulation. More work should be dedicated to simulating the surface fluid boundary in details, for instance a boundary that varies with the pressure could be used to better simulate the operation of a backpressure valve.

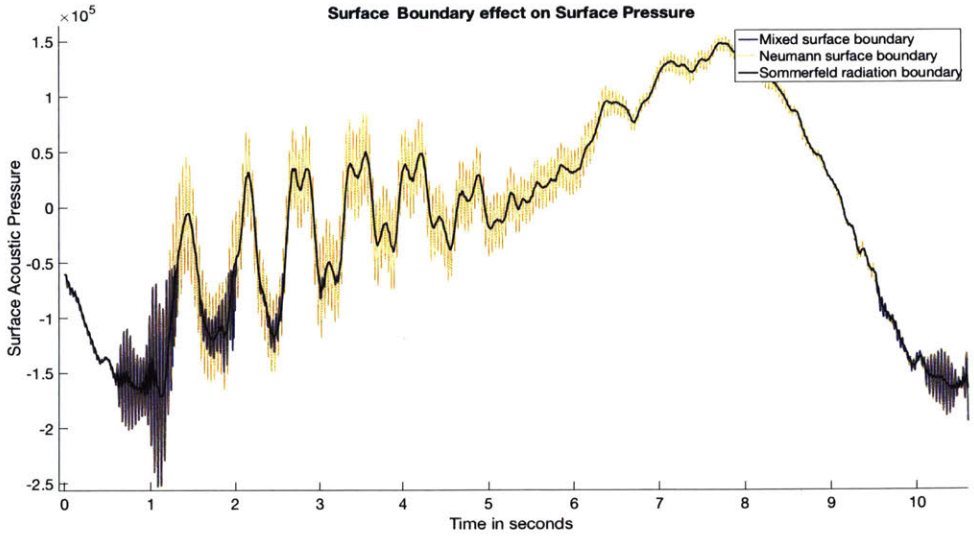

Figure 4-4: Effect of the surface boundary condition of the surface pressure. the non reflective boundary gives a smoother signal since there is no reflected wave. On the other hand the Neumann boundary (constant velocity) reflects every acoustic waves. The mixed boundary acts like a sommerfeld boundary above a set pressure and a Neumann below it.

4.5 Summary

In the context of oil wells, looking at the acoustic pressure field in the fluid system is a novel approach to infer and diagnose the operating characteristics of the pump. Digital pressure sensors can be placed at the top of the well and/or at various position along the rod string to infer useful pump condition. Specifically, the pressure at the surface can be evaluated and used as a diagnostic tool to complement or replace the strain measurement in the steel rod. This is an important point and it was decided to further explore the potential of using the pressure as a diagnostic tool by first gathering and interrogating field data followed by designing an experimental setup to assess the influence of various parameters on the pressure field of the system.

Chapter 5

Design of a Laboratory Scale Acoustic Pump system

While ideally experiments and real time measurements would be done on a real oil well, several limiting factor severely restrict that option. First it is expensive to place instruments downhole. The environment is harsh with high temperatures ($100°C$ and upward), high pressure, corrosive and abrasive liquid, vibrations, etc. Connecting those sensors with several miles of cable is also highly challenging as it requires a large number of connectors. Thus such approach is rarely attempted, most measurements are taken at the top of the well; these measurements are then used, in conjunction with empirical models, to infer and to explain/rationalize events occurring at the bottom.

The scaling approach has been successfully used in various fields such as aerospace and ocean engineering to design and implement scaled-down test rigs for quantifying the operations of vehicles and components. This is done through establishing a set of key non-dimensional parameters that characterize the pertinent physical processes underpinning the operation of the engineering devices. Such an approach is taken to first establishing the set of non-dimensional parameters characterizing the operation of rod-pump system followed by proposing the design of a scaled-down laboratory system in which a selected set of non-dimensional parameters are maintained. The details on the design of such a scaled-down laboratory rod-pump system for experimental

assessment of its operation is presented in this Chapter.

5.1 Methodology

As motivated in the beginning of this chapter, the goal was to design an experimental bench top model that would be able to replicate the dynamic acoustic effects created by the system. The experiment was designed and scaled but was not built. We will focus on scaling the acoustic aspects of a real well, and not its rod dynamics. This is a novel approach and the experiment is designed in stages of increasing complexity in order to ever improving the similitudes of the operating characteristics of a representative well.

This experiment would also allow one to evaluate the effect of various components in the well on the pressure signal propagation, helping us to reconstruct the source signal created by the pump. The effect of non ideal conditions such as gas interference and fluid pound could also be assessed.

5.2 Scaling the System

The scaling of the acoustic system was done in the same manner as the scaling of the rod system. We started using the simplified pressure wave equation in which the key terms are retained.

$$\frac{\partial^2 P}{\partial t^2} = c_f^2 \frac{\partial^2 P}{\partial x^2} + \Lambda_P \frac{\partial (v_{fluid}(x,t) - v_{rod}(x,t))^2}{\partial x} \tag{5.1}$$

5.2.1 Reduced frequency and non linear damping

We will scale the wave equation by normalizing the position x using the well length l, the time t using the driving period T. The pressure is non dimensionalized by $\rho_f v_{rod}^2$ and we assume the rod velocity is uniform along its length so v_{rod} is not a function of x. $(v_{fluid}(x,t) - v_{rod})$ becomes v_{rel}^* with $v_{rel}^* = (v_{fluid}(x,t) - v_{rod})/v_{rod}$. Doing so

we obtain the following equation in terms of non-dimensinal time and position:

$$\frac{\partial^2 p}{\partial t^{*2}} = \left(\frac{c_f T}{l}\right)^2 \frac{\partial^2 p}{\partial x^{*2}} + \left(\frac{\Lambda_P T^2}{\rho_f l}\right) \frac{\partial (v_{rel}^*(x,t)^2)}{\partial x^*} \tag{5.2}$$

From the wave equation for the fluid, the following non-dimensional parameters can be extracted:

$$\Pi_{f1} = \frac{c_f T}{l} \tag{5.3}$$

$$\Pi_{f2} = \frac{\Lambda_P T^2}{\rho_f l} \propto \frac{\Lambda_P T}{\rho_f c_f} \tag{5.4}$$

Since the experimental well is shorter than a real well, we have to decrease the period T and/or the sound velocity c in our experiment. The non linear damping coefficient which depends on the geometry of the obstacles on the rod string. Numerically since we will use a plastic pipe $c_f \approx 250 m/s$ we actually find that Λ_P has to change by 20%.

5.2.2 Reynolds number

We also wish to scale the fluid flow regime in order to retain the loss generation characteristic of a turbulent flow.

$$\Pi_{f2} = \frac{\rho_f V_f D}{\mu} \tag{5.5}$$

5.3 Experimental considerations

For practical considerations, it was decided to use water as a working fluid. While gas may be added later on, water will still be the main solvent. The well number 1 from Sandia's laboratory experiment [8] will be used as a reference.

5.3.1 Pipe length and material

The pipe length and material are chosen in order to keep Π_1 constant. The well length has to be shorter as it is impractical to use thousand of meters of pipe. 30m was chosen as most tubing is in increments of that length.
The pipe will be made of PVC and not steel in order to reduce the fluid sound velocity in it (cf Appendix C) by a factor of 6. However this will introduce extra damping from the plastic deformation, this damping will be measured experimentally and is not applicable in a real well. Upon setting the experimental well length and sound velocity, we now obtain the actuating frequency we should use. The pipe diameter will be about 10mm (based on availability), this is a compromise as a smaller pipe is less practical to use but the flow rate is lower and the system needs less power to pump the fluid.

5.3.2 Actuator and Pump Design

The actuator has to be able to move the pump in a sinusoidal motion, at a given amplitude and with a given maximum velocity. It is sized in order to provided the necessary power. As we have seen in the previous chapters, we have decoupled the pressure into two types of pressure, static and dynamic. The static pressure is manually adjusted by tuning the backpressure valve and the dynamic pressure is computed using the model. The pressure at the pump surface is the sum of both pressures. We can immediately deduce the power necessary to actuate the pump knowing the pump velocity, pressure and cross sectional area. The system is designed to use less than 100W of power.

The rod string is not simulated here, instead we directly actuate the pump and suspend it between springs in order to recreate the rod system dynamics and recreate the "chopped sinusoidal" waveform of the plunger. A hydraulic cylinder placed between 2 springs with a calculated stiffness in order to match the scaled system resonating frequency will be used as a pump. It will be driven by an electric motor (a drill). A backpressure valve placed at the end of the tubing allows the user to scale

the rod stretch, i.e. the larger the system pressure, the more the spring will compress before the piston starts moving. External check valves simulate the pump ball valves. Since the pump is acoustically compact (the acoustic wavelengths are much longer than the pump) we can place those valves outside the pump.

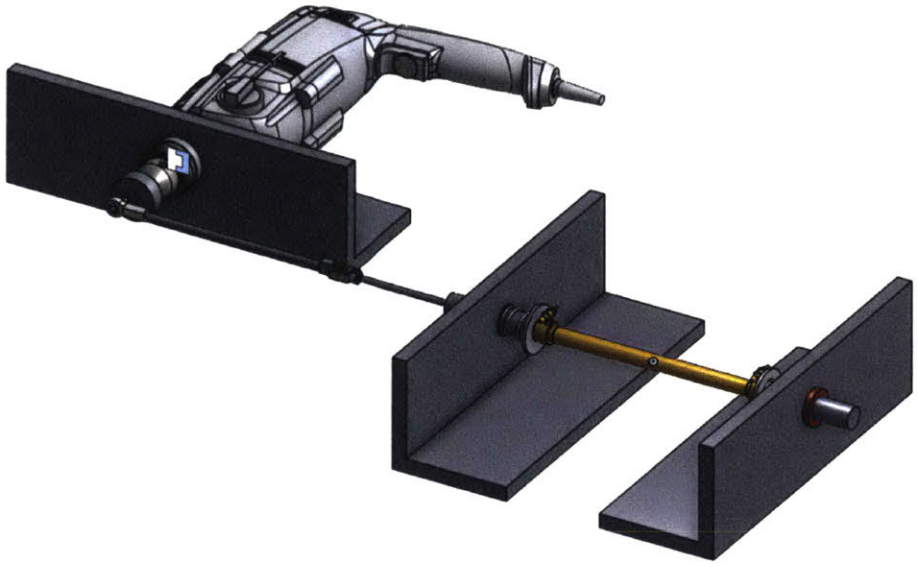

Figure 5-1: Scaled down pump CAD design with the hydraulic cylinder in yellow suspended between two springs

5.3.3 Rod String

A rod string can be added in the tubing. It will not be used to actuate the pump and is only here to recreate the non linear acoustic damping. That rod string will be actuated in order to fine tune the relative velocity between it and the fluid. The couplers/centralizers number and size are key variables to scale Λ_P. In the scaled-down experimental set up, the rod string will be a thin steel tube with teflon centralizers along its length to minimize solid friction.

5.3.4 System Overview

The experiment will be designed with a decoupled pump and rod. The main actuator will be placed behind the pump for precise direct-drive control. The rod movements

will be controlled by a different motor in order to assess the damping effect of the rod on the acoustic signal. The system layout is described in Figure 5-2.

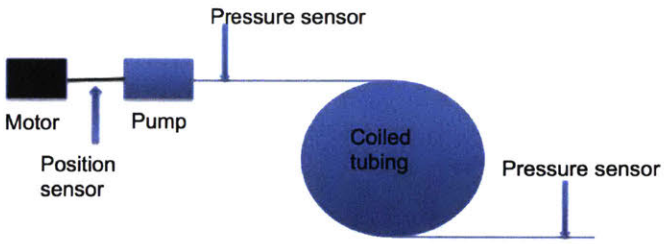

Figure 5-2: System experimental layout

Table 5.1: Scaling Summary

	Length	Rod Diam	Tubing Diam	Plunger Max Vel
Reference well	900m	19mm	57mm	1.3m/s
Scaled Experiment	30m	3.8mm	12mm	1.1m/s

5.3.5 Experimental Planning

The experiment should be constructed and implemented in phases with ascending level of complexity as illustrated in Figure 5-3. This will allow one to identify each individual contribution and to establish the traceability of each parameter on the strength of the acoustic signal.

The first step is to get the basic system operational and calibrate all the sensors and the pump actuator. The precise speed of sound in the plastic tube will be measured, along with the pump acoustic characteristic.

The second step will simulate an ideal well with top check valve boundary condition for the fluid, and the effect of the rod string on the pump acoustic signal.

The final step will assess the effect of gas in the fluid, and how it modifies the acoustic signal as it propagates in the fluid gas medium. If deemed necessary this step will also include a new pump design that will be a miniature 3D printed rod pump that could be actuated by a precise linear electric motor (voice coil) in order to replicate data gathered in the field.

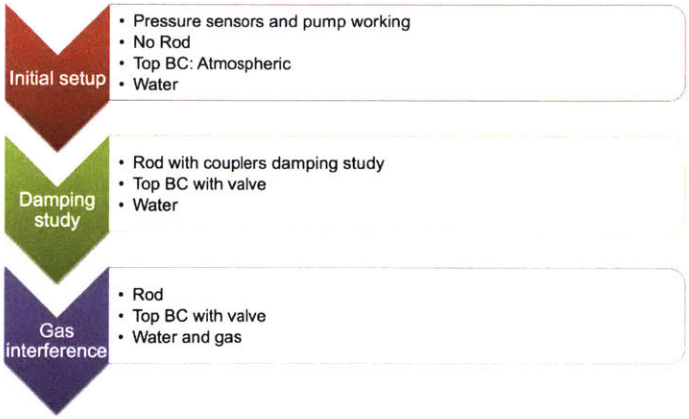

Figure 5-3: Experiment planning

5.4 Summary

The experiment would have allowed us to determine what are the limits of this technology (using the surface pressure measurement to infer downhole condition). The extent to which gas in liquid attenuates the propagating pressure wave, the sensitivity of the acoustic signal to the pump movement could both be studied with that setup. We would have also been able to formulate a transfer function that quantifies the acoustic filtering created by the movement of centralizers and couplers in the tubing.

Chapter 6

Field Data and Results

6.1 Introduction

Two sets of data were used, the first one was data acquired in the early 1990's by Sandia National Laboratory. They instrumented several wells and their data serves as a start to assess the model, specifically the stress analysis of the rod. However Sandia acoustic data was found to be incomplete in most of their instrumented wells so it was decided to acquire a new set of data specifically to assess the results from the acoustic analysis of the fluid-rod system. Surface stress and pressure were measured on a dozen wells of various types at various locations in Oklahoma.

6.2 An assessment of the Model using Sandia National Laboratory data

Six wells were instrumented by the Sandia team. Out of those wells, only 2 wells were used. Well 1 data is complete and well 3 data is almost complete with only the surface pressure sensor information missing. The other wells were not used either because they have a fiberglass rod string which is beyond the scope of this research or because the available data is incomplete or of poor quality to the extent that it is not useful to interrogate further.

Table 6.1: Sandia's Wells 1 and 3 dimensions

Well	Sandia 1	Sandia 3
Pump depth	830m	2814m
Plunger size	38.1mm	57.1mm
Period	5.45s	15.4s
Stroke length	218cm	777cm
Centralizers/couplers	190	375
Motor power	15kW	75kW

6.2.1 Pump card analysis

By convention, the results are displayed as a load vs displacement. The top surface chart has higher loads as it includes the rod weight in addition to the fluid weight, and is displayed above the pump chart. The oscillations on the top chart are due to the mass spring system behavior of the rod. The frequency of those oscillations is different on the upstoke and the downstroke as the mass of fluid lifted is lower on the downstroke. The pump chart oscillations reflects the presence of fluid acoustic waves as an incompressible fluid would lead to a perfectly rectangular pump chart. A typical user would be mostly interested in the maximum and minimum loads on the surface card, and in the shape and amplitude of the pump card. The surface loads allow one to evaluate fatigue and system sizing while the pump card is used to diagnose various pump issues.

Well 1

The stress match between the model and the measured data is excellent on the short well, Sandia 1. This is a relatively simple well with no tapering and no gas. We can estimate the measurements error in stress at about 5% for a typical load cell. The error in position is however much larger especially at the pump because we have a high temperature environment and the accelerometer sensor is integrated for a long period of time, thus the drift can be significant. Figure 6-2 details key variables from the model, the plunger displacement and velocity, the rod stretch (rod string length

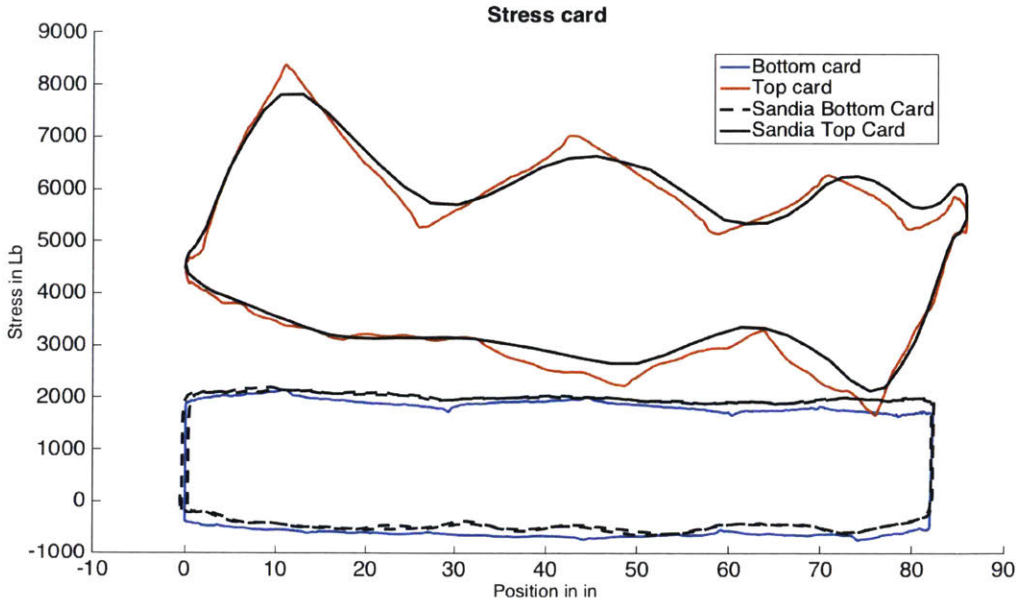

Figure 6-1: Pump chart for Sandia's well 1

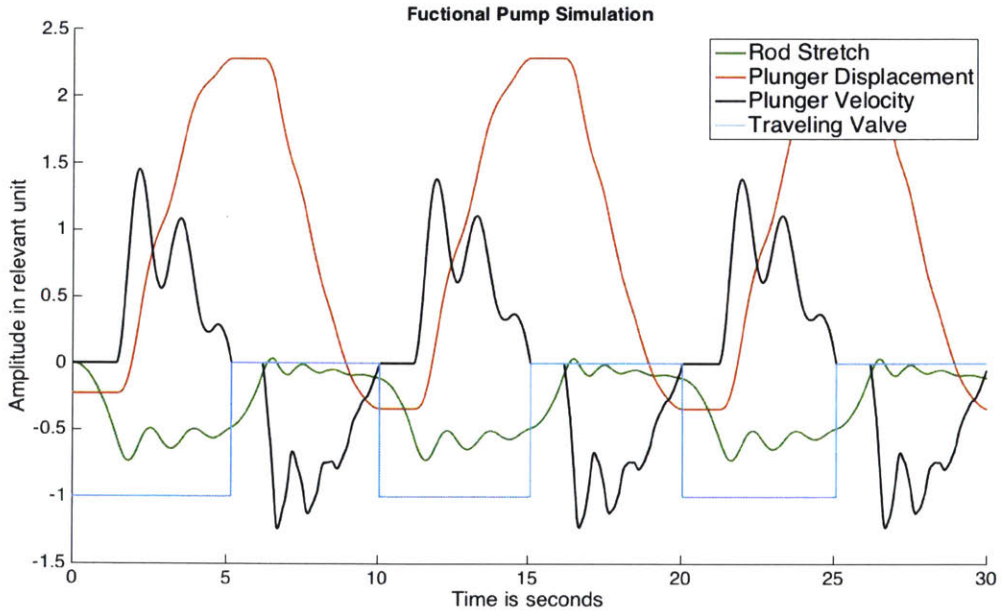

Figure 6-2: Well 1 analysis. The plunger oscillations during up and downstroke are visible as well as the associated rod strech

normalized by resting length) and the position of the traveling valve (-1 is closed and 0 is open). The plunger oscillates during both upstroke and downstroke at the system natural frequencies as calculated previously. Since the lifted load is larger on the upstroke the frequency is lower.

Well 3

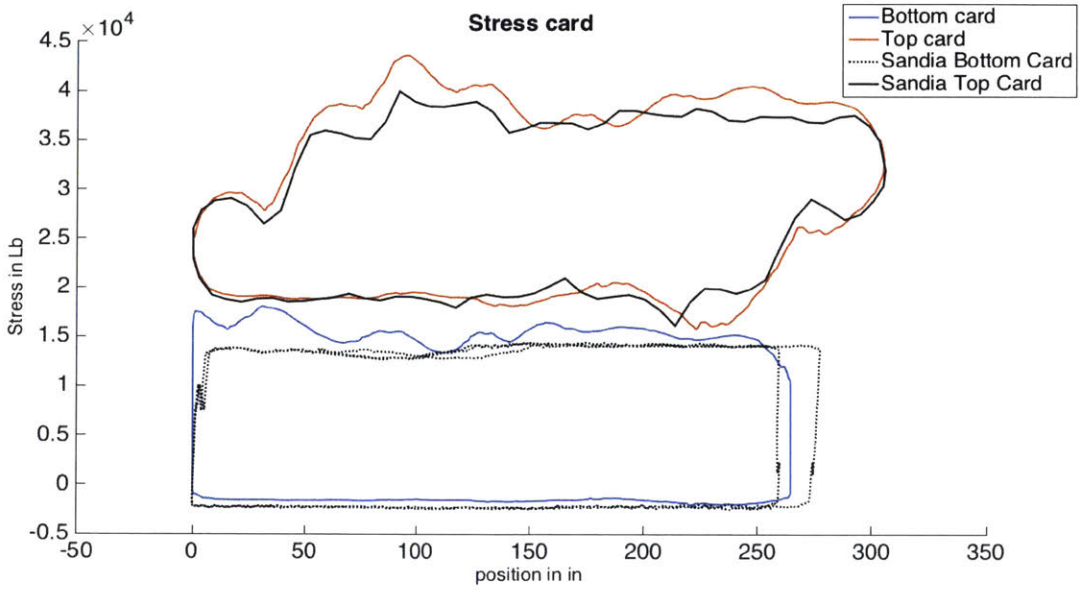

Figure 6-3: Pump chart for Sandia's well 3

For Sandia well 3, presented in Figure 6-3, the stress calculation are within 10% of the measured data. As explained previously the pump amplitude was different stroke to stroke because of integration drift. Measurements from a set of two strokes are shown in figure 6-3: one corresponding to the longest stroke (about 275 inches at the pump) and the other to the shortest stroke (about 255 inches). The model calculated stroke is between those two extreme measurements.

6.2.2 Pressure analysis

Well 1

Looking at the pressure right above the pump, in Figure 6-4, we see a good agreement between what is measured and what is computed.

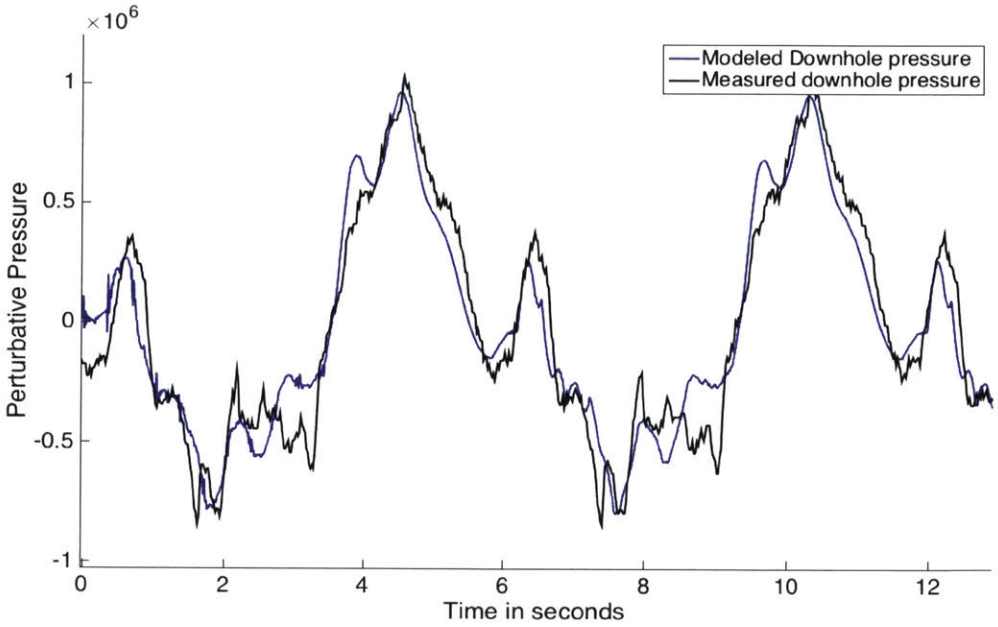

Figure 6-4: Pressure above the pump, well 1

6.3 Field Data Acquisition and Results from Wells in Oklahoma

In order to understand in details the acoustic pressure propagation it was decided to gather additional experimental data. To understand the role of gas fraction on the system acoustic response wells with various gas content and wells with gas lock were instrumented. Those measurements allowed the modeling of gas lock and reservoir coupling.

Table 6.2: Oklahoma Well 49-3 and 52-1 dimensions

Well	49-3	52-1
Pump depth	3263m	722m
Plunger size	31.8mm	38.1mm
Period	10.65s	9.54s
Stroke length	280cm	168cm

6.3.1 Data acquisition system

The surface card was gathered by a contractor using the Echometer instrumentation system. The surface pressure data was gathered by either a 200psi or a 667psi sensor with a bandwidth of 900Hz at a sampling frequency of 500Hz. A labview interface connects the sensor to a 12bit DAQ 6000 series from National instruments.

6.3.2 Gas lock

Several key off design conditions were observed during the field measurements. One of the key condition is called gas lock and it is analysed in this section.

Gas lock criteria

If the barrel contains too much gas, the barrel pressure will not be high enough at the end of the downstroke phase to open the traveling valve, this effect is visualized in Figure 6-5. This effectively locks the pump and prevents any pumping. If we define the compression ratio CR as the minimum barrel volume (at the bottom of the stroke) divided by the maximum barrel volume (at the top of the stroke). We can establish a criteria for when gas lock will occur. The compression in the barrel is assumed isentropic thus the heat capacity ratio γ links changes of volume and pressure according to the thermodynamic relation $PV^{\gamma} = constant$. In this case the value for natural gas is used. The pressure above the plunger is the sum of the hydrostatic pressure in the tubing and the surface back pressure which is set by the operator. The pressure at the barrel inlet is the sum of the casing pressure and the hydrostatic pressure created by the fluid level in the casing. We are in gas lock when:

$$P_{tubing} + \rho_f g l > \frac{P_{casing} + \rho_f g l_{casing}}{CR^{\gamma}} \tag{6.1}$$

Most often the tubing pressure is much smaller than the downhole hydrostatic pressure, and we usually get into gas lock when the casing fluid level is low thus we obtain the following simplified equation:

$$\rho_f g l > \frac{P_{casing}}{CR^{\gamma}} \tag{6.2}$$

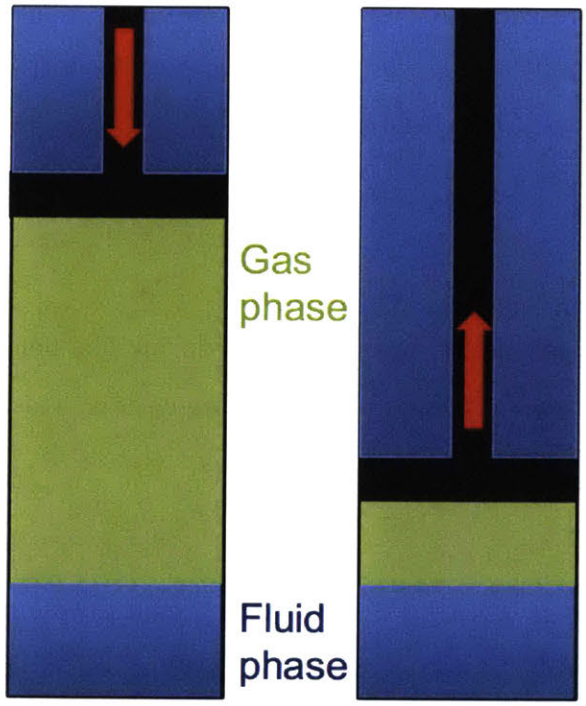

Figure 6-5: Schematic of a gas lock situation in the pump, liquid is in blue and gas in green. In this example there is about 75% gas on the upstroke in this case the compression ratio is about 4 which is not enough to open the traveling valve

To prevent gas lock one could increase the casing pressure but usually the range of adjustment is limited. Instead by changing the pump spacing (pump resting position) the compression ratio (usually in the 100-300 range) can be increased by a factor of 2 or 3. Since the CR is raised to the powerγ this almost eliminates the likelihood of a gas lock happening.

Gas lock analysis

One of the wells, NMU49-3, was found to go into frequent gas lock cycles, about every 3 minutes. This well was used as a case study for gas lock and the design and operating characteristics of Well NMU49-3 are given in Table 6.2. Four time interval are visible in figure 6-6:

- 60-100s: increasing liquid fraction in the plunger, pump is leaving gas lock phase

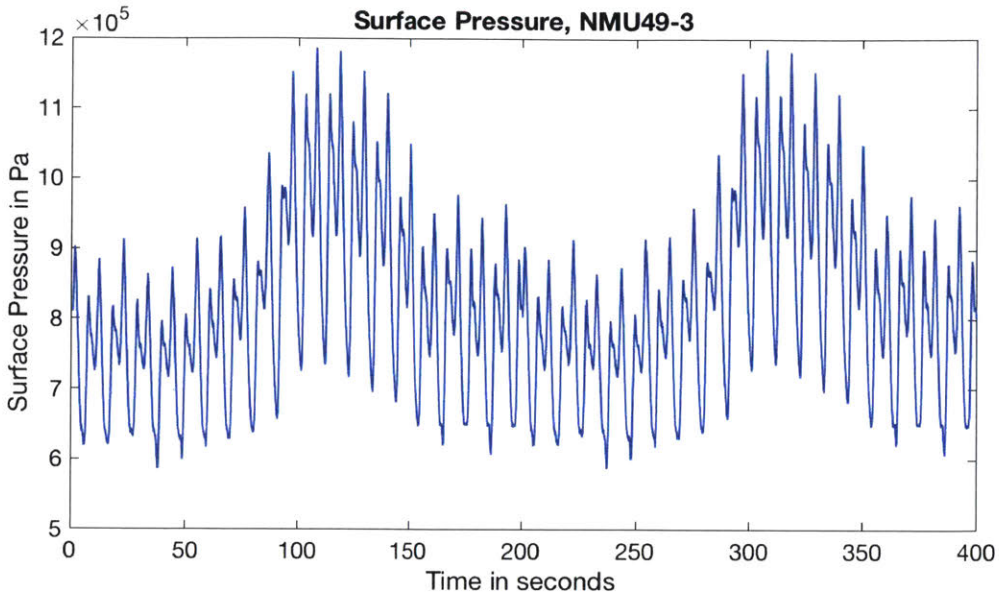

Figure 6-6: Recorded pressure at the surface of well NMU49-3

- 100-130s: barrel full of liquid, efficient pumping
- 130-140s: decreasing liquid fraction in the plunger, pump going into gas lock
- 140-250s: pump is in gas lock, pressure is slowly dropping due to plunger leakage

The leakage model developed using the fluid equations in Chapter 3 explains how the plunger can exit gas lock. As fluid leaks across the plunger, the barrel is progressively filled with fluid. This increases the compression ratio CR since only the gas is compressible, and using equation 6.2, the well will exit the gas lock phase and start pumping.

During the gas lock phase the mean pressure also decreases with time. This is also explained by the leaking flow across the plunger. Understanding pump leakage allows the modeling of low frequency mean pressure changes (frequencies below the driving frequency).

6.3.3 Gas fraction and tubing stretch analysis

To prevent gas lock, the pump barrel needs to have a minimum amount of fluid in it. On the other hand a full pump with no gas often means that the system is not

pumping fast enough and the well can provide more fluid. An ideal system pumps the exact amount of fluid provided by the oil reservoir. A practical way to do this is to keep the pump operating with a small gas fraction (0-20%, thus there is a need to monitor the pump gas fraction).

We will use the well ECU52-1 as a case study to understand the effect of gas fraction on the acoustic surface pressure signal. Our measurements also show the well tubing string was un-anchored.

ECU52-1 pump chart

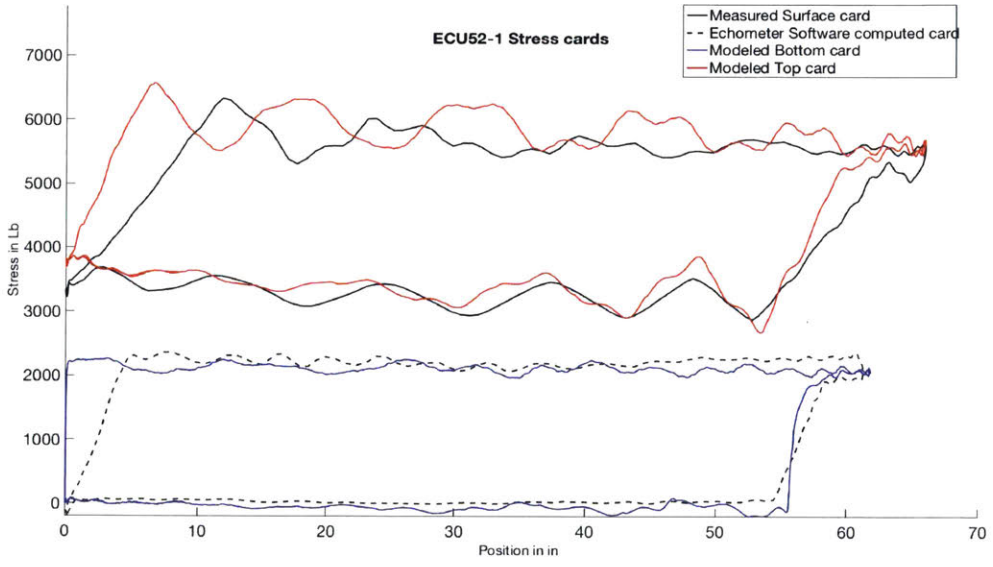

Figure 6-7: ECU52-1 surface and pump cards

The cards in Figure 6-7 are in general agreements in that the modeled and the measured surface card oscillations have the same frequency and same mean values. The pump amplitude and mean stress levels are also matched. The key difference is observed at the beginning and at the end of the stroke. The modeled load build up/ decay is much faster than the measured one so that the simulated pump card looks like a rectangle instead of the measured parallelogram. This happens because the tubing is either un-anchored or the anchor failed and detached, thus the whole tubing string stretches at each load change applied to the plunger. This is a well

known phenomena in the oil well service field that is not modeled in this work [12].

ECU52-1 acoustic signal

We observe a strong correlation and a good match between the measured and the modeled acoustic signals in Figure 6-8. The high frequency noise is due to a rusty backpressure valve and was easily audible at the well site. The downstroke section of the signal matches well the measured signal (5 to 9s). However the upstroke simulation does not matches as well (0-5s). This is expected since the surface chart in Figure 6-7 also matched well for the downstroke compare to the upstroke. Without taking the damping effect of tubing stretching into account, the shock load on the pump on the upstroke is much higher creating a stronger dynamic effect. On the downstroke the 10% gas fraction already creates a damping effects thus tubing stretch has a smaller effect.

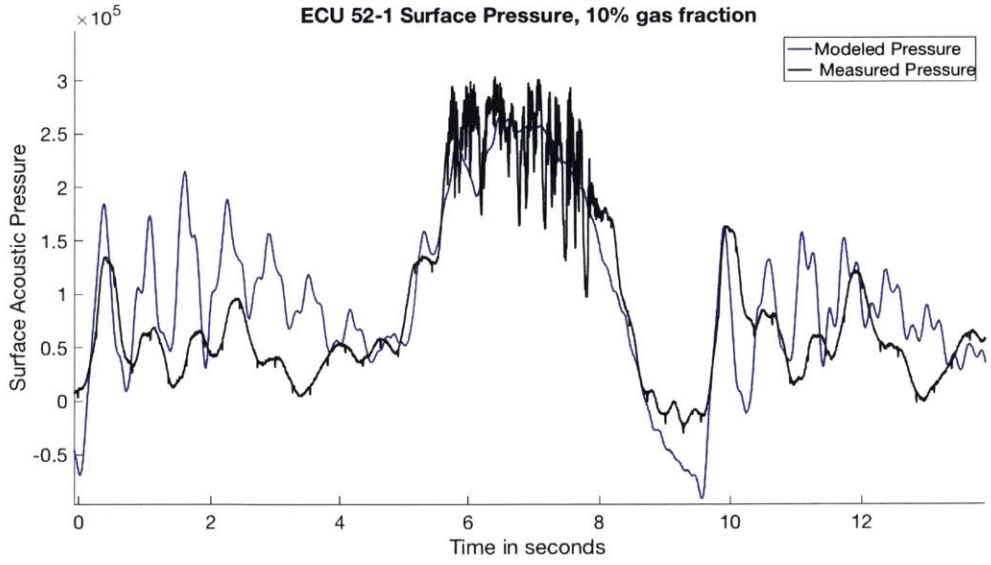

Figure 6-8: Well ECU 52-1 modeled and measured pressure signal with 10% gas in the pump

While doing a numerical parametric analysis on the gas fraction, it was noticed that the acoustic signal corresponding to the downstroke phase greatly varied. This computed phase variation with gas fraction is shown in Figure 6-9. This was confirmed experimentally by plotting each stroke of Well 52-1 surface signal.. The surface stress

analysis that was measured simultaneously also indicates that each stroke had a different pump gas content with a gas fraction ranging from 0 to almost 60 %.

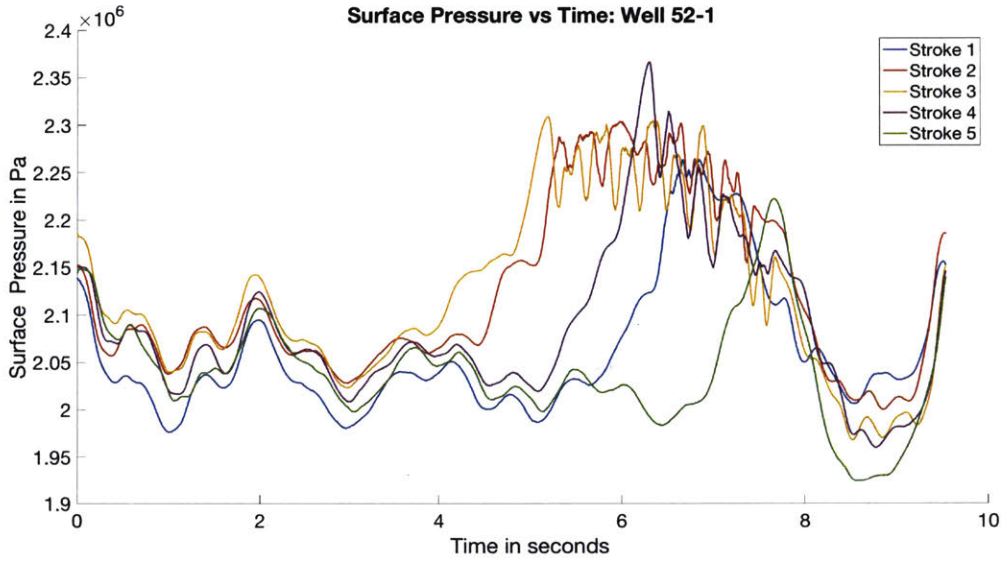

Figure 6-9: Evolution of the measured surface acoustic signal, each stroke of the recorded signal was superposed

Using the model the following plot in Figure 6-10 was generated, showing the strong similarities with the recorded signal and showing the physical fidelity of the model.

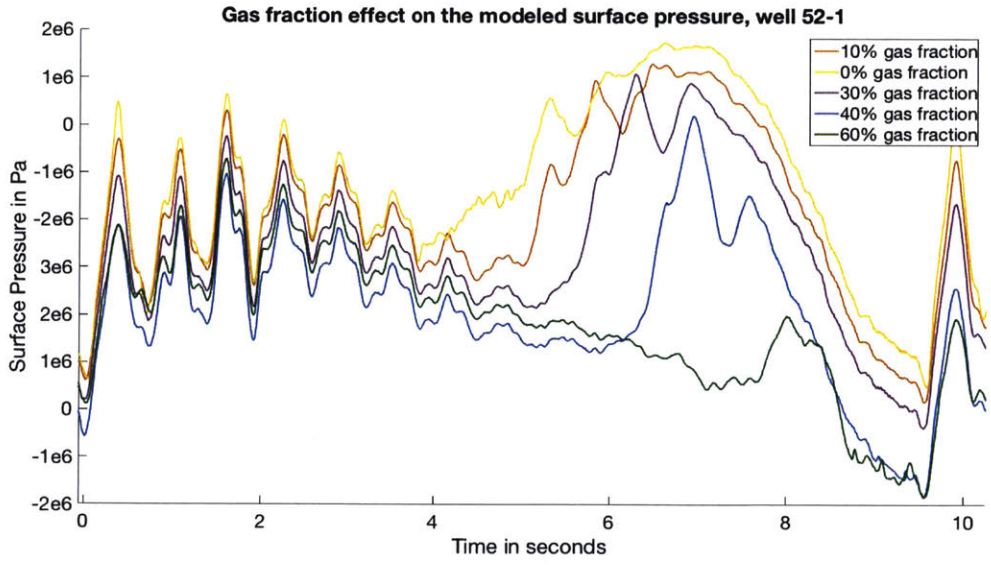

Figure 6-10: Effect of gas fraction in the pump on the surface acoustic signal, each stroke of the generated signal was superposed

Generalised gas fraction analysis

In order to quantify the phase difference created by the varying gas fraction content of the pump, it was necessary to understand the source of that time delay before carrying out any non-dimensional analysis. The following analysis is quasi-steady and does not take into account dynamic effects, therefore its accuracy increases if the system driving frequency is significantly lower than the resonating frequency.

Increasing the gas fraction in the pump delays the pressure build up in the barrel during the downstroke phase as seen in Figure 6-11. This means that the traveling valve will open at a later time. When the valve opens the pump immediately starts pumping thus creating a pressure pulse. The downstroke phase delay was plotted in Figure 6-12 for three different wells.

The volumetric gas fraction is defined as volume of gas in the pump over the pump volume, which can be re-written as the length of the gas phase Δx over the pump amplitude $\mathcal{A}_{pump}$ such that $gasfraction = \frac{\Delta x}{\mathcal{A}_{pump}}$. Since the traveling valve opens during the middle part of the downstroke the pump motion can be assumed to be linear. $\mathcal{A}_{top}$ is the amplitude of the rod motion at the top of the rod string, the well surface (polished rod), and is imposed by the unit kinematic.

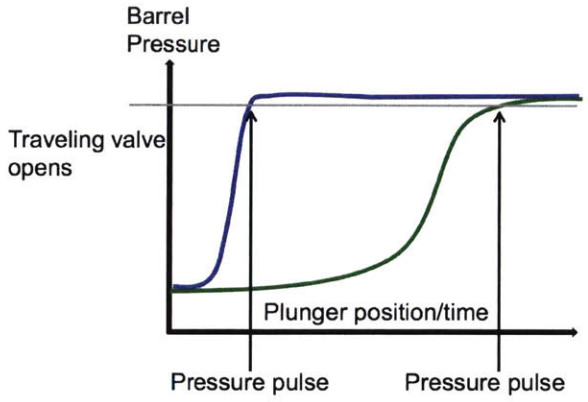

Figure 6-11: Barrel pressure with and without gas during the downstroke

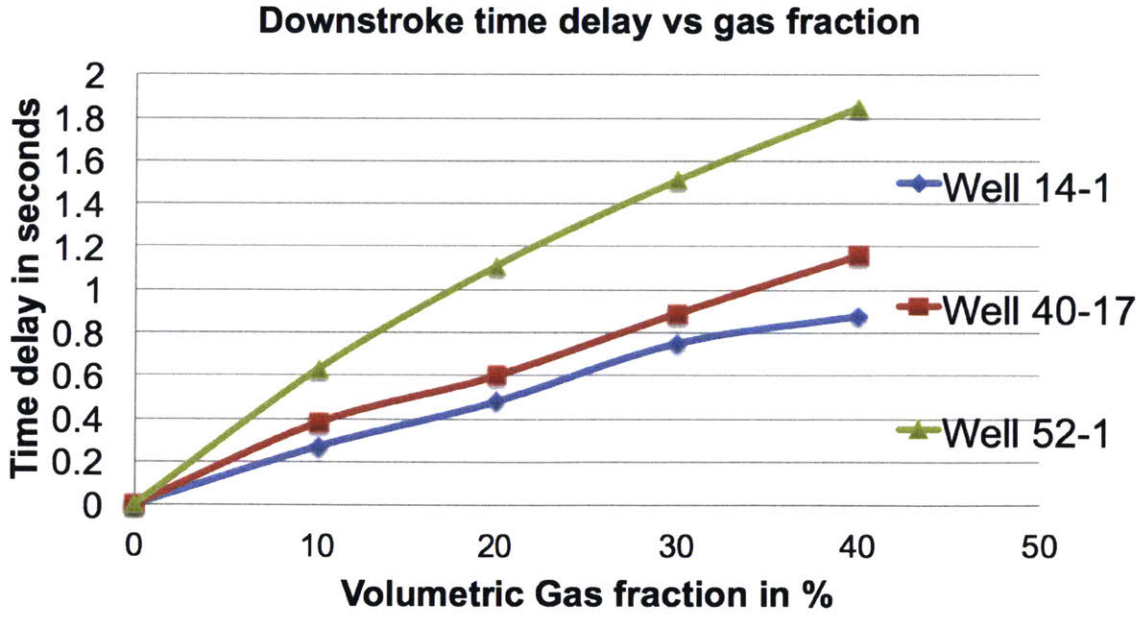

Figure 6-12: Time delay vs gas fraction for 3 wells, each well is associated with a different slope

The surface amplitude is larger than the pump movement as the rod has to stretch and unstretch at every cycle. The pump amplitude is approximated to be the polished rod amplitude minus the rod stretch due to the fluid weight $\frac{F_0}{k}$.

$$\mathcal{A}_{pump} = \mathcal{A}_{top} - \frac{F_0}{k} \tag{6.3}$$

When the pump ingest low pressure gas during an over pumping condition, Δx is also approximately equal to the displacement between the top of the pump stroke and the position at which the valve opens. This is justified by the high compression ratio (typically 80 to 400) thus the gas volume is negligible after compression compare to the fluid volume inside the pump. This extra compression that has to be done before opening the traveling valve is associated with a time delay Δt. The pump average velocity when moving is $\frac{2\mathcal{A}_{top}}{T}$ with T is the system period. We obtain the gas fraction based on Δt in equation 6.4.

$$gasfraction = \frac{2\Delta t}{T} \frac{1}{1 - \frac{F_0}{k\mathcal{A}_{top}}} \tag{6.4}$$

In Figures 6-13 and 6-14 we compare the time delay computed with 3 different methods, the model, the formula, and the experimental measurements.

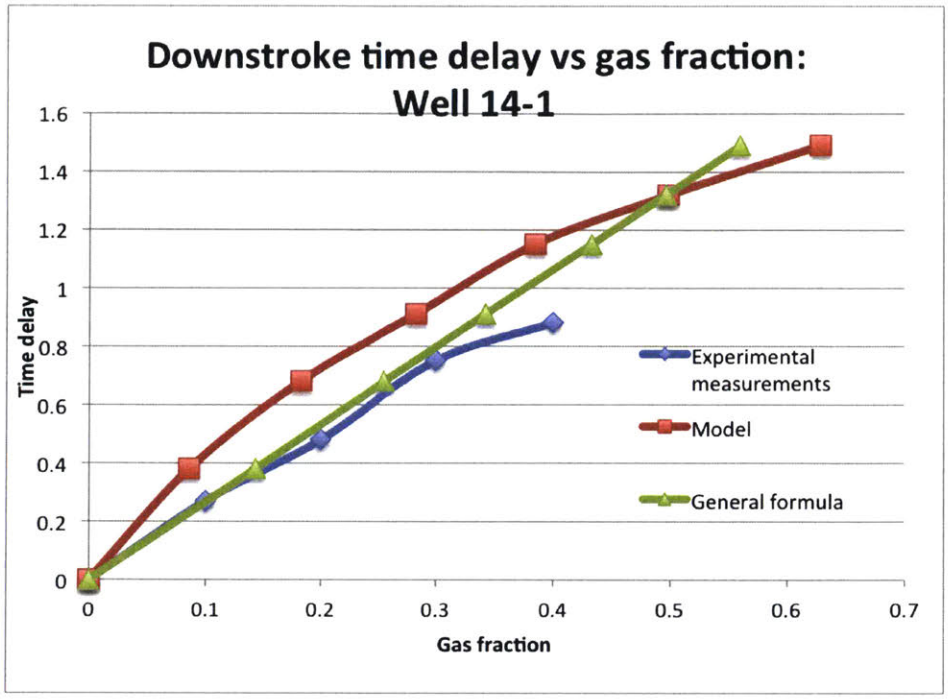

Figure 6-13: Time delay vs gas fraction computed using three different methods on well 14-1. The general formula in equation 6.4 is compared to the recorded signal and the signal generated by the model

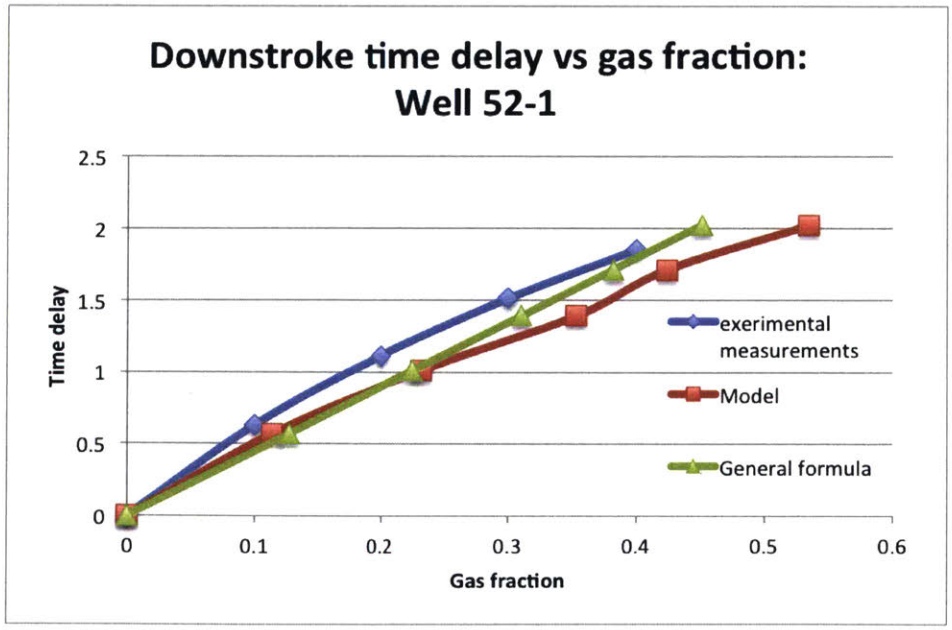

Figure 6-14: Time delay vs gas fraction computed using three different methods on well 52-1. The general formula in equation 6.4 is compared to the recorded signal and the signal generated by the model

We infer from Equation 6.4 that the physically rational parameter to scale the downstroke time delay is $\frac{T}{2}(1 - \frac{F_0}{k\mathcal{A}_{top}})$. Armed with this scaling parameter, the data in Figure 6-12 can be recast in terms of the normalized time delay against the gas fraction percentage to yield a near universal curve. This is shown in Figure 6-15. In addition the corresponding results from the rod-pump system model are shown alongside with the data and the agreement shows the physical consistency between both the field data and the model developed here. As expected the slope is 1.

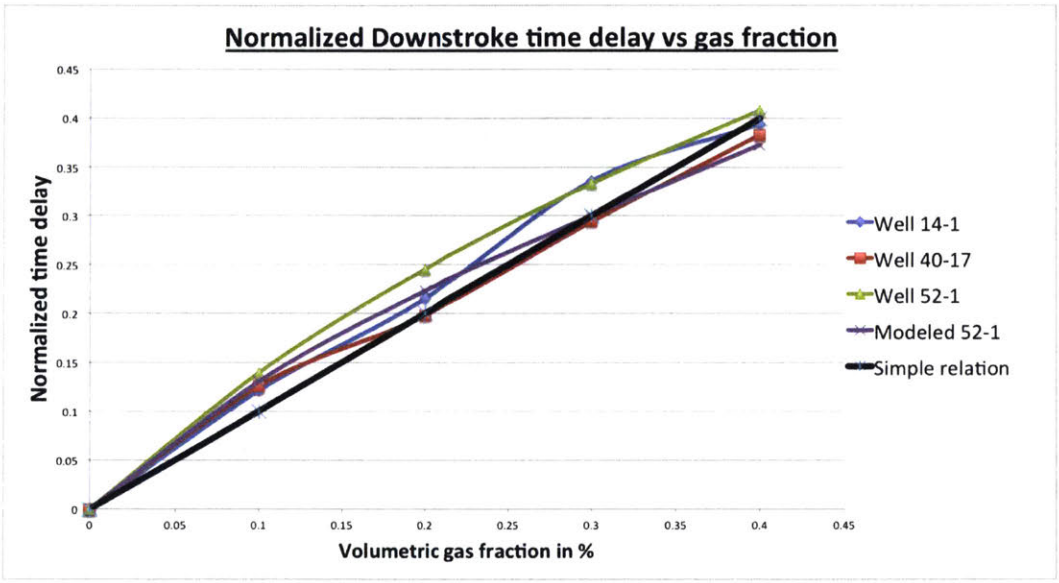

Figure 6-15: Normalized time delay vs gas fraction for 3 wells using the measurements and using the model

Using the formula in equation 6.4 allows a user to instantly estimate within a error margin of about +/-5% the amount of gas in the pump of any oil well using a simple surface acoustic measurement.

6.4 Well-reservoir coupling

Well reservoir coupling was briefly assessed. It was assumed that the reservoir provide a constant flow to the well. This is a simplistic assumption and more advanced models like a diffusion model or a numeric reservoir model could be used instead. The well in this example is constantly pumping. In an ideal world, a well would automatically

detect that there is no more fluid to pump and would slow down or shut off for a specific length of time. That time would depend on both the well and the reservoir properties. The diagram of the flow are shown in Figure 6-16.

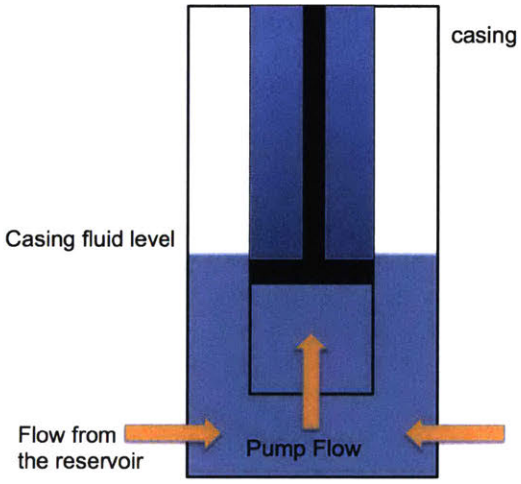

Figure 6-16: Flow diagram at the bottom of the well

In Figure 6-17, a low flowing well is being pumped faster than it can replenish, thus the level in the casing drops at every stroke until the well is empty. At the same time the gas fraction in the pump increases.

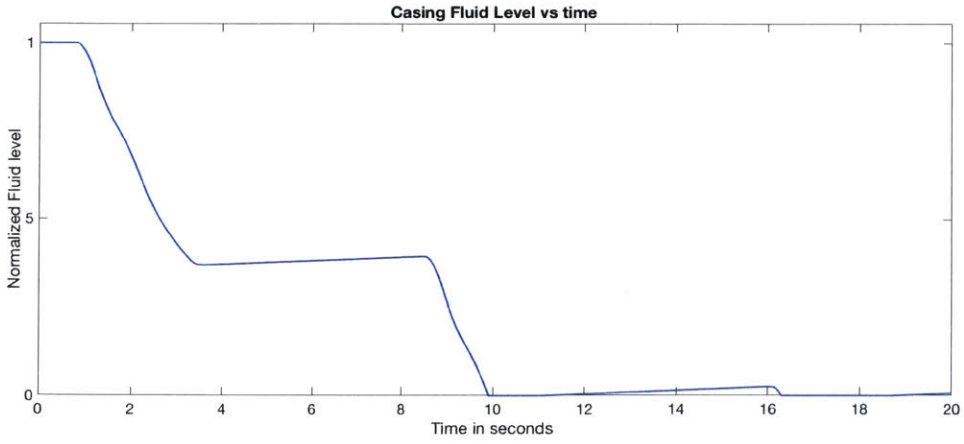

Figure 6-17: Example of casing fluid level in a low flowing well

6.5 Current limitations

Backpressure valve

The next key improvement to the model will be a more realistic surface boundary condition than the current ideal valve model. Since simple direct acting ball-spring backpressure valves are used in the field, there can be more than 100% pressure difference between a fully open valve and a valve that is barely cracked open. This is illustrated in the Figure 6-18. Direct acting valves are used on the field due to their low cost and robustness compare to pilot acting valves.

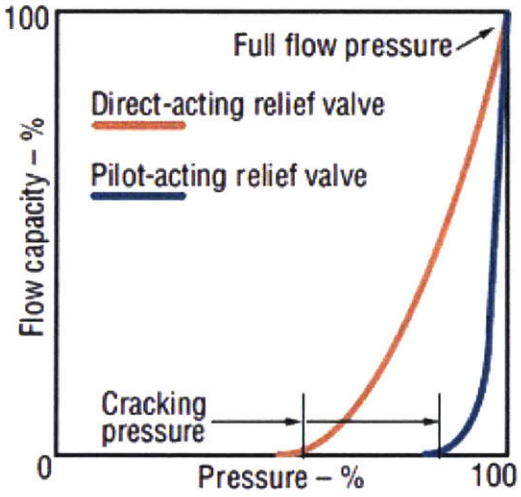

Figure 6-18: Valve pressure vs flow, from http://www.hydraulicspneumatics.com/

Leakage effect

While the leakage is calculated and its effect on the gas fraction is taken into account, the effect it has on the pressure drop in the tubing is not yet evaluated. In reality the tube is pressurized and leaking fluid will cause a drop in the mean pressure.

Solid friction at the pump

Many measured surface pressure signal contain more high frequencies than the modeled signal. It is hypothesised that this is due to the non smooth movement of the

pump occurring when solid frictions affects the plunger movement. In theory solid friction will increase acceleration spikes at the pump thus creating an additional high frequency acoustic signal.

Other model limitations

Valve leakage, un-anchored tubing and rod tapering effects are not yet taken into account to model the pump acoustic signal.

6.6 Summary

A strong signal was measured on most instrumented wells, confirming the calculation that any gas existing in the well will be dissolved in the brine water pumped. Depending on the gas and brine concentration, the gas can come out of solution once a specific pressure is reached. Since most wells use a backpressure valve to pressurize the well the gas is not an issue.

The model provide great results for the rod stress analysis and highly encouraging results for the surface pressure analysis. While not all existing effects are currently modeled, the most important downhole conditions can currently be captured. The next steps should be to develop the proper signal processing method to extract the useful information for the pressure signal.

Chapter 7

Summary and Conclusion

7.1 Summary

This thesis assesses the characteristics of a rod pump system and the dynamic effects that occur in the system. Fluid and mechanical models are used to evaluate both the pump/surface cards and the pressure in the tubing. The pressure at the tubing surface is analyzed to understand the effect of various pump off-design conditions. Simulations done using a numerical approach were compared to existing measurements as well as new ones done in the field. A scaled down experiment was designed and could be built in future work to recreate any pump condition. It was found that generally modeled pump and surface cards are in good agreement with measured cards. Acoustic pressure signal amplitude is difficult to model as the pressure signal is highly sensitive to plunger acceleration, however the signal phase matches well the measured signal. A parametric assessment shows that the mechanical system is weakly coupled to the acoustic system, i.e. the pressure waves in the tubing do not affect the system except at the pump. At the pump boundary, assuming the well is either compact (fluid is a lumped mass) or purely acoustic (infinitely long well with no reflected waves) is sufficient to give a good estimate of the well cards. However the acoustic system is strongly coupled to the mechanical system, the downhole pump is not the only source of pressure waves, rod tapering is also key and rod centralizers/couplers can also be important in certain cases.

In terms of the research questions posed in Chapter 1, we have to a large extent addressed the followings:

- Defined the attributes of a rod pump system both mechanically in the rod string but also acoustically in the tubing
- Determined the key non dimensional scaling parameters
- Determined the influence of the mechanical system on the tubing pressure and the resulting pressure waves
- Quantified the effect of various off-design pump condition on the acoustic tubing pressure

As of to-date the main sources of damping on a rod pump have been assessed and a model for loss estimation formulated. The system movement and stress is evaluated for various cases, ranging from shallow to deep wells and compared with the provided experimental data. A simplified analytical model was initially used to understand the system and was later replaced by a more advanced fully non linear computational model. The analytical model was then used as a baseline to assess the accuracy of the computational model. A universal scaling parameter was defined and used to compare the effect of gas interference on the pressure signal for any well. Several off design effects such as gas interference or gas lock have been modeled and reservoir coupling was briefly analyzed; however there are many more existing effects such as tubing stretch or fiberglass rods that are not part of this work.

7.2 Conclusion

The model formulated in this thesis is based on the physical processes and dynamics in the rod pump system. This not only yields a model in accord with the field data but also enables one to rationalize why the field data look the way it is in terms of the physical processes setting the rod pump system operation; in addition, the model provides the physical basis for formulating the scaling rule for the rod pump

system. Thus these are not the only original contributions of the thesis work thus far but they also provide enablers to begin designing and planning a scaled-down experimental set up implementable in laboratory environment. The hypothesis that a finite set of measurables at the top of the well can be used to define the downhole conditions has been proven true for at least some downhole conditions. Specifically, a simple pressure measurement at the top can be used to infer gas interference using the universal scaling established in this work. The implication of this hypothesis/idea is that it provides a powerful basis to develop a diagnostic tool for a broad class of generic artificial lifts for vertical as well as non-vertical wells.

7.3 Recommendation for Future Work

The future research tasks will consist of two threads:

- The implementation of the experiment to :
  - Understand the relation between pump velocity and its acoustic signature
  - Evaluate the damping effect of gas bubbles on the pressure waves
  - Evaluate the non-damping effect of rod centralizers and couplers
  - Experimentally decouple the various acoustic effects
- Further refinements to the rod-pump system model to include
  - A fully coupled distributed damping that varies with rod position and time
  - A diagnostic code that uses the pressure signal to evaluate the pump velocity
  - Effect of multiphase Fluid

Several key theoretical elements still have to be evaluated and understood better. The various damping terms need to be refined, especially the damping created by the flow across the pump.

The flow acoustic characteristics during the downstroke phase have to be evaluated. In that situation the flow is going upwards while the rod string is going downwards, this create a new acoustic damping term.

The effect of gas (bubbles or layers) is still not known, this may be studied both experimentally and theoretically.

Appendix A

The Wave Equation

The movement of the pump downhole is described by the wave equation A.6 and subjected to two boundary conditions at the top and at the bottom of the well. We assume the rod has a radially uniform stress distribution, a constant area cross section, and is homogenous. When the rod is tapered the equation is solved by section. K is the polar radius of gyration of the steel rod (function of the rod geometry) and ν is the Poisson's ratio of the rod. We also assume the rod stays within the elastic limits of the material such that Poisson's Law (see equation A.1) holds (i.e. the stress in the rod is proportional to the rod strain); this can be verified after calculation by comparing the maximum stress in the rod and the elastic limit of the material. It is also assumed that all the forces occurring at the surface of the rod are proportional to the rod velocity and the wetted area.

$$\sigma = E\frac{\mathrm{d}\xi}{\mathrm{d}x} \tag{A.1}$$

The force balance on a small section of rod yields to the wave equation A-1 that describes the dynamic of the rod pump system.

$$\rho dx\pi R_{rod}^2\frac{\partial^2\xi}{\partial t^2} = Edx\pi R_{rod}^2\frac{\partial^2\xi}{\partial x^2} + \lambda''2\pi R_{rod}dx\frac{\partial\xi}{\partial t} + \rho dx\pi R_{rod}^2 g \tag{A.2}$$

In accordance with the Love theory we incorporate the lateral inertia effect $\lambda''2\pi R_{rod}dx\frac{\partial\xi}{\partial t}$ which is a dispersive term. It takes into account ν,the Poisson's ratio of the rod, and

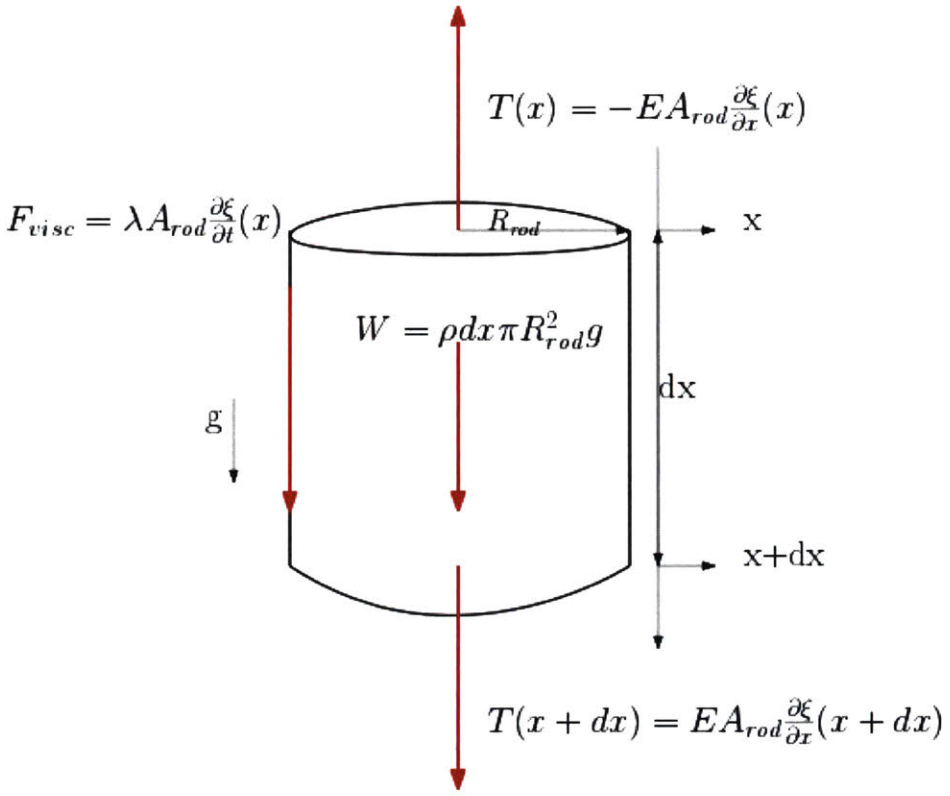

Figure A-1: Force Balance on an infinitesimal rod element of length dx

K the polar radius of gyration of the rod. The origin of that term can be found by using Hamiltonian mechanics to do an energy balance on the rod [2]. c is the sound velocity of compressive waves in a long rod given by $c = \sqrt{\frac{E}{\rho}}$.

$$\frac{1}{c^2}\frac{\partial^2 \xi}{\partial t^2} = \frac{\partial^2 \xi}{\partial x^2} + \left(\frac{\nu K}{c}\right)^2 \frac{\partial^4 \xi}{\partial x^2 \partial t^2} + \frac{2\lambda''}{R_{rod}\rho c^2}\frac{\partial \xi}{\partial t} + \frac{g}{c^2} \tag{A.3}$$

This equations contains a dissipative term with a dissipative coefficient λ' and a dispersive term with a dispersive coefficient $(\nu K)^2$.

To determine the conditions for which the effects associated with wave dispersion can be neglected, we resort to the dispersion relation from the exact theory, the Love theory and the wave equation theory shown in Figure A-2. The ordinate in Figure A-2 is the velocity $\bar{c}$ given in equation A.4 and the abscissa is the normalized wave number $\bar{\gamma}$ given in equation A.4. In equation A.4 c_0 is the phase velocity in the absence of dissipation and dispersion, and $K = \frac{R_{rod}}{\sqrt{2}}$ for a cylindrical rod. In general c has a functional dependence on the wave number γ.

$$\bar{c} = \frac{c}{c_0}$$
$$\bar{\gamma} = K\nu\gamma \tag{A.4}$$

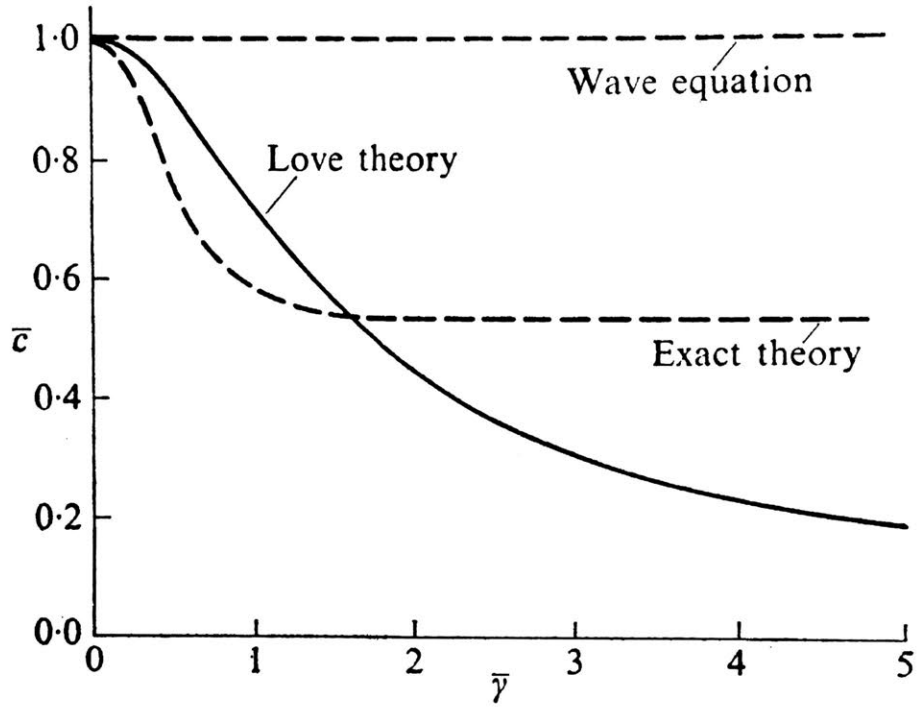

Figure A-2: Dispersion curve for Love's rod theory, wherein radial-inertia effects are included

From the results shown in figure A-2, dispersion effects can be neglected if $\bar{\gamma} < 0.3$ so that $c \approx c_0$, i.e. the phase velocity is essentially independent of the frequency.

For example, with a steel rod of radius 2.54cm (1 inch)we find the frequency corresponding to $\bar{\gamma} = 0.3$ is $f = 92kHz$ where we have used $\gamma = 2\pi fc$

The frequency to be encountered in the rod-pump system is well below the threshold value of 92kHz; thus the approximation that the phase velocity c is essentially independent of the frequency is good so that we can neglect the dispersive term.

The sound velocity is also a function of the stress in the material, or its elongation

(both are linked with the Poisson's law). One can show that the sound velocity in the rod is:

$$c = c_0 \left(\frac{L}{L_0} \right)^2 \tag{A.5}$$

Where L is the length of the rod under tension, L_0 is the length of the rod at rest, and c_0 is the sound velocity in the rod at rest. Since the rod only stretches by a few % to stay within the elastic domain of steel (avoiding irreversible damage), we can assume $\left(\frac{L}{L_0} \right)^2 \approx 1$.

The sound velocity in the rod is thus a weak function of the stress and that dependence will not be taken into account in the following formulation and analyses. For a long rod where the diameter is smaller than the wavelengths that travel in it, the sound velocity c is $c = c_0 = \sqrt{\frac{E}{\rho}}$. The frequency being examined are in the order of 1Hz which leads to a corresponding wavelength of about 6000m which is several orders of magnitudes larger than the rod diameter, thus confirming the validity of the formula. We also use $\lambda = \frac{2\lambda'}{R_{rod}\rho}$.

Equation A.3 reduces to:

$$\frac{\partial^2 \xi}{\partial t^2} = c^2 \frac{\partial^2 \xi}{\partial x^2} + \lambda \frac{\partial \xi}{\partial t} + g \tag{A.6}$$

Appendix B

Models comparison

B.1 Accuracy check

A few study cases have been setup in order to compare both results and check every aspects of the models:

- a system with no distributed damping and a fixed end: λ=0,Z=0
- a system with no distributed damping and a mass attached at the end: λ=0,Z=jwm
- a system with no distributed damping and damping at the end: λ=0,Z=R
- a semi infinite rod with distributed damping: $\lambda \neq 0$

The first case compare the wave propagation in both models and eliminate the question of implementing a complex bottom boundary condition. The second and third cases respectively verify the implementation of an admittance and a resistance at the bottom. The last studied case verifies the propagation of a wave in a rod with distributed damping. Analytically we obtain:

$$\xi(x,t) = A_0 e^{k'' x} cos(\omega t - k' x) \tag{B.1}$$

Numerically this was done by simulating a rod much longer than the critical damping length $\frac{1}{k''} = \frac{\lambda' c}{\sqrt{2}} \frac{1}{\sqrt{1+\sqrt{1+\left(\frac{\lambda' c^2}{\omega}\right)^2}}}$ and implementing a basic non reflective boundary.

Any reflected wave will be damped out and will not influence the rod oscillation in the studied section.

The results for two key cases are shown bellow. An infinite rod is studied first to show that the core of the numerical model is valid, then the results with the full boundary to show that the boundary condition can be accurately modeled.

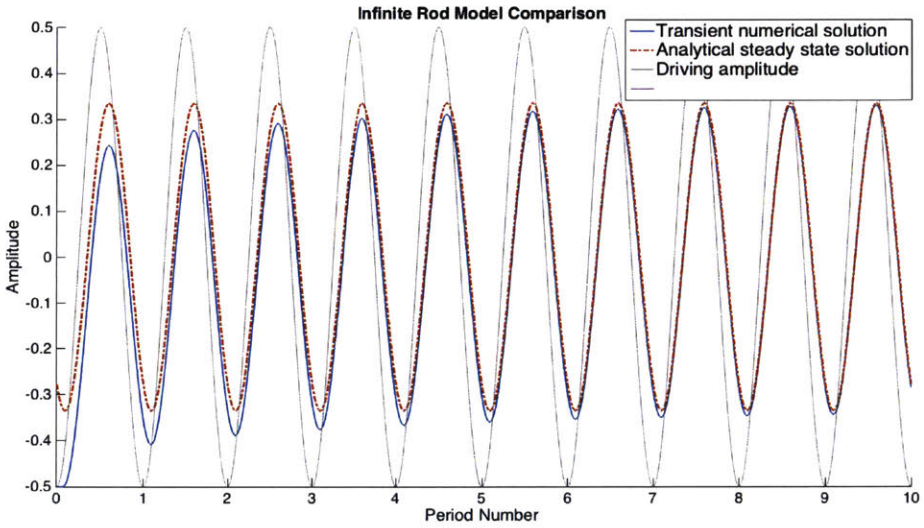

Figure B-1: Infinite rod simulation

As expected the numerical model transient solution converges to the analytical model steady state solution.

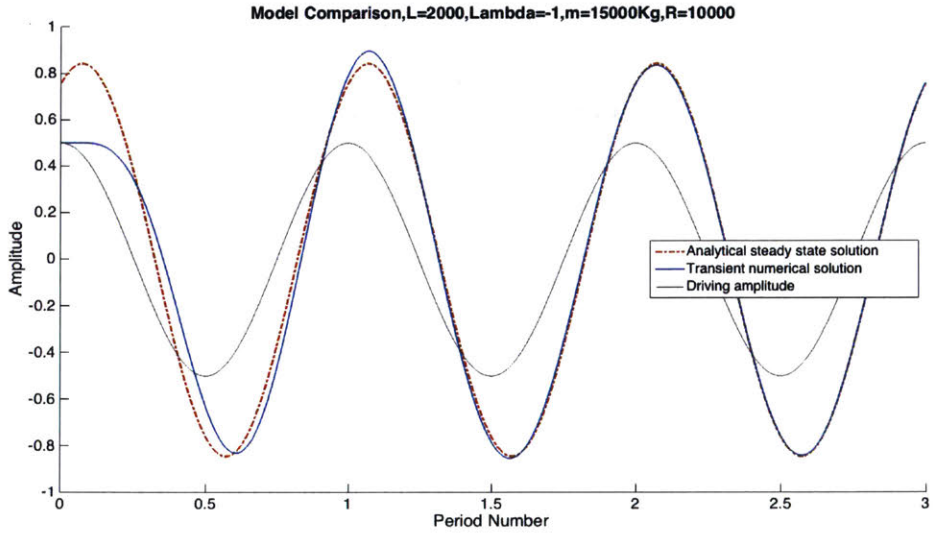

Figure B-2: Fixed mass and damping linear simulation

In every case, it can be seen that both models give what will we consider to be identical results with less than 0.1% difference in both amplitude and phase. It was also observed than increasing the numerical grid size increases the accuracy of the numerical model.

Appendix C

Pressure Propagation Considerations

C.1 Curvature effect

The effect of a curved pipe on its acoustic characteristics has been studied previously [10]. The authors studied the influence of the ratio of the pipe radius divided by its radius of curvature on the acoustic properties. It was found that if $\frac{R_{pipe}}{R_{curvature}} << 1$ the curvature has no effect on the sound propagation.
In an oil well, that ratio is in the order of 10^{-3} so we can neglect the curvature effect on the pressure waves.

This is one of the main reason the acoustic method is of great interest to study deviated well, the well orientation has no effect on the pressure waves.

C.2 Pipe stiffness effect and wave equation

When a pressure wave is propagating in a pipe, it locally deforms the pipe. Experimentally it has been observed that the speed of sound in the pipe is greatly reduce when the pipe is flexible. We will show in this section how to evaluate the speed of sound in the fluid as a function of the pipe properties.

A is the pipe area, V_f the fluid velocity and ρ_f its density. A mass balance between x and x+dx in a pipe section gives us:

$$\frac{\partial}{\partial x}\left(V_f(x,t)\rho_f(x,t)A(x,t)\right) + \frac{\partial}{\partial t}\left(\rho_f(x,t)A(x,t)\right) = 0 \tag{C.1}$$

We also know the relation between the change of density and pressure using the fluid compressibility β:

$$\frac{\partial \rho_1}{\partial t} = \chi_S \rho_f \frac{\partial p}{\partial t} \tag{C.2}$$

And we introduce the pipe distensibility D_s, which is isentropic:

$$D_S = \frac{1}{A}\left(\frac{\partial A}{\partial P}\right)_S \tag{C.3}$$

The new first order mass balance which also takes into account the fluid compressibility and the wall distensibility is now:

$$\frac{\partial V_f(x,t)}{\partial x} + (D_S + \beta)\frac{\partial p(x,t)}{\partial t} = 0 \tag{C.4}$$

We obtain the wave equation using the following linearized Euler equation:

$$\rho_f \frac{\partial V_f(x,t)}{\partial t} = -\frac{\partial p(x,t)}{\partial x} \tag{C.5}$$

The pressure wave equation is:

$$\frac{\partial^2 p(x,t)}{\partial t^2} - \frac{1}{\rho_f(\chi_S + D_S)}\frac{\partial^2 p(x,t)}{\partial x^2} = 0 \tag{C.6}$$

The sound velocity is now a function of D_S with $c = \frac{c_0}{\sqrt{\rho_f D_S}}$, c_0 being the sound velocity in the fluid only.

Using a hoop stress balance we find D_S as a function of the pipe inner radius R_p,

and its thickness h. This is expression is only valid if $h << R_p$.

$$D_S = \frac{R_p}{Eh} \tag{C.7}$$

Appendix D

Numerical Scheme

D.1 Discretization

The wave equation studied here contains a dissipative term, and only a very small range of frequencies travel across the rod. Thus it is important to find a numerical scheme that preserve the damping characteristics, while the dispersive accuracy is not of great importance. There are various existing scheme that can be used, and they model dispersive and dissipative effects with different levels of accuracy. A scheme that has little numerical damping was used and is described in the next section

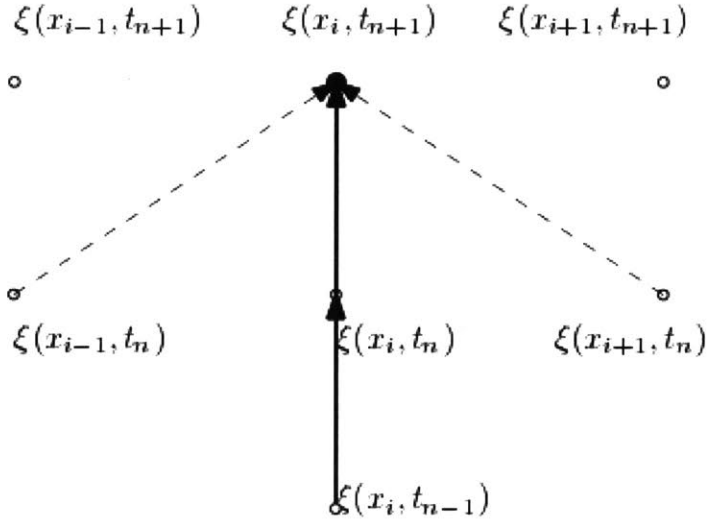

Figure D-1: Numerical Scheme

The wave equation is discretized using a second order central difference method.

If we denote i the position on the x axis with $x_i = i\Delta x$ and n the position on the time axis with $t_n = n\Delta t$. s is the CFL factor with $s = c\frac{\Delta t}{\Delta x}$, c being the sound speed in the material. We can discretize the first derivatives in space using a second order method.

$$\frac{\partial \xi_i^n}{\partial x} = \frac{\xi_{i+1}^n - \xi_{i-1}^n}{\Delta x} \tag{D.1}$$

Using the same method we obtain the second order derivative:

$$\frac{\partial^2 \xi_i^n}{\partial x^2} = \frac{\xi_{i+1}^n - 2\xi_i^n + \xi_{i-1}^n}{\Delta x^2} \tag{D.2}$$

We use the exact same methods for the time derivative.

The wave equation becomes::

$$\xi_i^{n+1} = \frac{2(1-s^2)\xi_i^n + s^2\xi_{i-1}^n + s^2\xi_{i+1}^n - (1+\frac{\Lambda dt}{2})\xi_i^{n-1} - gdt^2}{(1-\frac{\Lambda dt}{2})} \tag{D.3}$$

This is written with matrices in Matlab to increase the algorithm speed.

D.2 Boudary Conditions

By applying Newton Second Law to the pump's plunger we have:

$$m_{pump}\frac{\partial^2 \xi(l,t)}{\partial t^2} = -EA_{rod}\frac{\partial \xi(l,t)}{\partial x} - g + F_{visc} - \Delta P(A_{pipe} - A_{rod}) \tag{D.4}$$

The viscous force F_{visc} is the damping force created by the thin lubricating fluid. The pressure forces depends on the upstroke or downstroke motion (position and direction of travel) and on the velocity as detailed previously.

At the top of the rod the displacement ξ_1^i is imposed for every time step i.
At the bottom of the rod, Newton Second Law is applied and discretized. Several force coefficient depends on the phase of the movement, i.e. upstroke or downstroke. The equation is here written for the upstroke.

$$\xi_{Nx}^{i+1} = 2\xi_{Nx}^{i} - \xi_{Nx}^{i-1} - \frac{EA_{rod}\Delta t^2}{m_{pump}\Delta x}(\xi_{Nx}^{i} - \xi_{Nx-1}^{i}) \\ -\Delta t^2 * g + \left(\frac{\Delta t^2}{m_{pump}}\right)(F_{visc} - \Delta P A_{plunger}) \tag{D.5}$$

The key difficulty here lies in the pressure difference across the plunger ΔP. While the pressure below is known, the pressure above the plunger includes the dynamic pressure term mentioned earlier. The only way to evaluate that term is to solve the full wave equation in the fluid and couple it with the rod wave equation at the bottom boundary, the plunger. This will be detailed in the following Chapter.

D.3 Rod Tapering

Most wells are build with a rod string that tapers as depth increases. Two or three rod diameters are common. At every area change there is a discontinuity in the rod impedance.

We know that displacement and force are preserved at a change of section. We note k the position at which the section changes we obtain, A_k the rod area before k, A_{k+1} the rod area after k, E the rod young modulus indexed in the same way. The stress is equal to the spacial derivative of the elongation and the + or - denote the left or the right spatial derivative.

$$\xi_k^i = \xi_{k+1}^i$$
$$E_k A_k \frac{\partial \xi_k^i}{\partial x}^{-} = E_{k+1} A_{k+1} \frac{\partial \xi_k^i}{\partial x}^{+}$$

The system is solved numerically using matrices with as many section changes as necessary.

Bibliography

[1] S. Gibbs, *ROD PUMPING: Modern Methods of Design, Diagnosis, and Surveillance*

[2] K. Graff *Wave Motion in Elastic Solids*,Dover publications, 1991

[3] J. Lighthill *Waves in Fluids*

[4] A. Pierce *Acoustics*

[5] E. Greitzer *Internal Flow*

[6] E. Kausel *Structural Dynamics*

[7] P. Morse, U. Ingard *Theoretical Acoustics*

[8] R. Cutler *Fluid Dynamics in Sucker Rod Pumps*, Sandia National Laboratories

[9] Y;S. Muzychka, M.M. Yovanovich *Unsteady viscous flows and Stockes's first problem*, International Journal of Thermal Sciences, November 2009

[10] S. Felix, JP. Dalmont. *Effects of bending portions of the air column on the acoustical resonances of a wind instrument*, 26 pages. 2012. hal-00643184v1

[11] http://www.globalspec.com/reference/78794/203279/html-head-chapter-2-the-components-of-the-sucker-rod-pumping-system

[12] J. Svinos, *Practical Rod Pumping Optimization*, ibook

[13] L.Hongtao, *Attenuation law of MWD pulses in aerated drilling*, Petroleum exploration and development, Volume 39, Issue 2, April 2012

[14] S. Huang, *Simulation of Surface Acoustics in Mud Pulse Telemetry Systems - Application to an Extended Reach MWD Telemetry Job at Sakhalin*, Schlumberger Journal of Modeling, Design, and Simulation, vol 3, June 2012

[15] S. N.Y. Gerges, *Muffler Modeling by Transfer Matrix Method and Experimental Verification*

[16] Y. Elnemr, *Acoustic Modeling and Testing of Exhaust and intake System Components*, Licentiate Thesis, KTH, 2011

[17] K. Brown, *Overview of Artificial Lift Systems*,Society of Petroleum Engineers, 9979,1982

[18] B. Neely, *Selection of Artificial Lift Method*,Society of Petroleum Engineers, 10337,1981

[19] J. Lea, *Selection of Artificial Lift*,Society of Petroleum Engineers, 52157,1999

[20] K. Palka, *Optimizing Downhole Fluid Production of Sucker-Rod Pumps with Variable Motor Speed*,Society of Petroleum Engineers Production Operations, 2009

[21] B.Alpert, *Nonreflecting Boundary Conditions for the Time-Dependent Wave Equation*, Journal of Computational Physics 180, 270-296, 2002

[22] N. Corbett, *A Symmetry Approach to an Initial Moving Boundary Value Problem Associated with the Wave Equation*, Canadian Applied Mathematics Quartely, Vol 18, Number 4, 2010

[23] L. Gaffour, *Analytical Method for Solving the One-Dimensional Wave Equation with Moving Boundary*, Progress in Electromagnetic Research, PIER 20, 63-73, 1998

[24] D. Appelo, *Non-reflecting Boundary Conditions for Wave Propagation Problems*, Licentiate Thesis, KTH, 2003

[25] S. Rienstra, *An introduction to Acoustic*, Eindhoven University of technology, 2015

[26] Z. Duan, *The prediction of methane solubility in natural waters to high ionic strength from 0 to 250c and from 0 to 1600 bar*, Eindhoven University of technology, Geochimica et Cosmochimica Acta, Volume 56, pp 1451-1460, 1992